Photoreflectance spectroscopy applied to semiconductors and semiconductor heterostructures*

JAN MISIEWICZ, GRZEGORZ SĘK, PIOTR SITAREK

Institute of Physics, Wrocław University of Technology, Wybrzeże Wyspiańskiego 27, 50–370 Wrocław, Poland.

The photoreflectance spectroscopy is presented as a powerful tool for the characterisation of semiconductor bulk and heterostructures. The advantages and possibilities offered by this electromodulation technique to investigate optical properties of a number of semiconductors and semiconductor structures, on which the modern electronic and optoelectronic devices are based, are reviewed. We discuss the application of the photoreflectance spectroscopy to study various properties of semiconductors, including the composition of multinary semiconducting compounds, carrier concentration, characteristic lifetimes of carriers, energies of trap states, distribution of the built-in electric field in homo- and heterostructures, the influence of perturbations such as temperature, strain and effects of growth, processing and annealing.

1. Introduction

Since its inception in 1964, modulation spectroscopy has proved to be a powerful experimental technique for studying and characterising the properties of bulk semiconductors, reduced dimensional systems (surfaces, interfaces, heterostructures, *etc.*), actual device structure and growth/processing. The basic idea of modulation spectroscopy is a very general principle of experimental physics. Instead of directly measuring an optical spectrum, the derivative with respect to some parameter is evaluated. This spectroscopy has been shown to be sensitive to critical point transitions in the Brillouin zone, with the resulting spectrum having sharp derivative-like features and little, if any, featureless background. Also, weak features that may have been difficult to observe in absolute absorption or reflection spectrum can be enhanced. Because of this derivative-like nature, a large number of sharp spectral features can be observed even at room temperature. In addition, information is also contained in the other experimental variables such as the modulation frequency, amplitude and phase.

The modulation can be easily accomplished by varying some parameter of the sample or experimental system in a periodic fashion and measuring the corresponding normalised change in the optical properties. It is possible to modulate a variety of parameters, including the wavelength of the incident beam, the sample tem-

---

*This is an invited reviewing paper.

perature, an applied stress or an externally applied magnetic and electric fields. In this paper we focus our attention on one particular contactless form of electric field modulation spectroscopy called photoreflectance. This is an alternative to the standard elctromodulation techniques, which jave not been used so widely because many of the more interesting samples are fabricated on semi-insulating substrates and thus present some difficulty in applying electric fields. Even if samples on doped substrates are available, the use of Schottky contacts or the electrolyte is required, which would etch away or substantially modify the device under study. Therefore we are basically intersted in electromodulation caused by photoinduced changes of the internal built-in electric field.
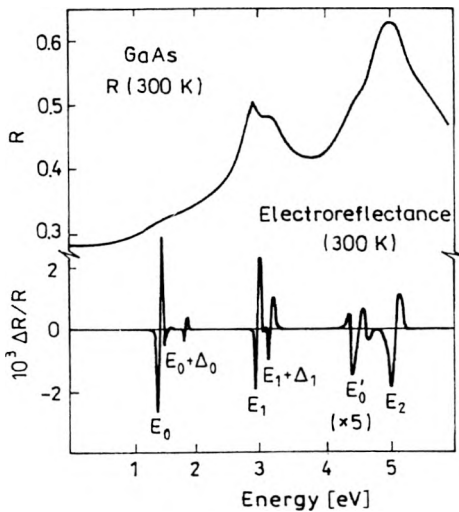

Fig. 1. Comparison of room temperature reflectivity and electric field modulated reflectivity (electroreflectance) of GaAs [1]−[3].

In Figure 1, the reflectivity R and electromodulation (electroreflectance − ER) spectra are compared for bulk GaAs at 300 K [1]−[3]. Whereas the reflectivity is characterised by broad features, the ER modulation spectrum is dominated by a series of very sharp lines with zero signal as a baseline. Notice that much of the broad featureless background of the reflectivity measurement is not present in the ER spectrum. Herein lies the power of the modulation spectroscopy: uninteresting background structure is eliminated in favour of sharp lines corresponding to specific transitions in the Brillouin zone. While it is difficult to calculate a full reflectance spectrum, this is not the case for modulation spectroscopy. For well-known critical points in the Brillouin zone, it may be possible to account for the line shapes in modulation spectrum [3]−[6].

In this paper, we review the possibilities and advantages of photoreflectance spectroscopy applied to investigation of different properties of semiconductor bulk, thin epitaxial layers and heterostructures. In Sec. 2 we start with a brief description of the experimental technique, followed by short fundamentals of the electromodula-

tion theory in Sec. 3. The particular applications of the photoreflectance spectroscopy are detailed in Sec. 4.

2. Experimental details

Modulation techniques including photoreflectance take advantage of the application of a small periodic perturbation to a physical property of the sample investigated. The change in the optical function (reflectivity or absorption) is only a small fraction of its unperturbed value, typically 1 part in 10^4 or less. The perturbation is usually extracted through the use of a lock-in amplifier tuned to the modulating frequency. This aspect of modulation spectroscopy is common to all techniques, including electroreflectance, photoreflectance, wavelength modulation, piezoreflectance and thermoreflectance. We will describe in more detail the photoreflectance technique.

Fig. 2. Schematic representation of photoreflectance apparatus [7].

The experimental apparatus for photoreflectance spectroscopy is shown in Fig. 2 [7]. The probe light is a monochromatic beam obtained from either a tungsten lamp or a quartz halogen source dispersed through a monochromator. The reflected probe beam is detected by a photomultiplier or a suitable photodiode. Modulation of the electric field in the sample is caused by photo-excited electron-hole pairs created by the pump source (laser or other light source) which illuminates the same spot of the sample and is chopped at certain frequency f_m. Most of the PR experiments have utilised a mechanical chopper with maximum several kHz. To achieve higher modulation frequencies up to 1 MHz an acoustooptic modulator can

be used [8]. The photon energy of the pump source is generally above the band gap of the semiconductor being investigated. The pump beam creates photo-injected electron hole pairs which modulate the built-in electric field of the semiconductor or semiconductor microstructure. The mechanism of the photoinduced modulation of the built-in electric field is explained in Fig. 3 for the case of an n-type semiconductor. Because of the pinning of the Fermi energy at the surface, there exists a space-charge layer. The occupied surface states contain electrons from the bulk. Photoexcited electron–hole pairs are separated by the built-in field, with the minority carrier (holes in this case) being swept towards the surface. At the surface, the holes neutralise the trapped charge, reducing the built-in field.

The light striking the detector contains two signals: a dc or average value $I_0 R$ (where I_0 is the intensity of the light impinging on the sample and R is the energetic reflectivity coefficient) and a modulated ac value $I_0 \Delta R$ varying with the frequency f_m
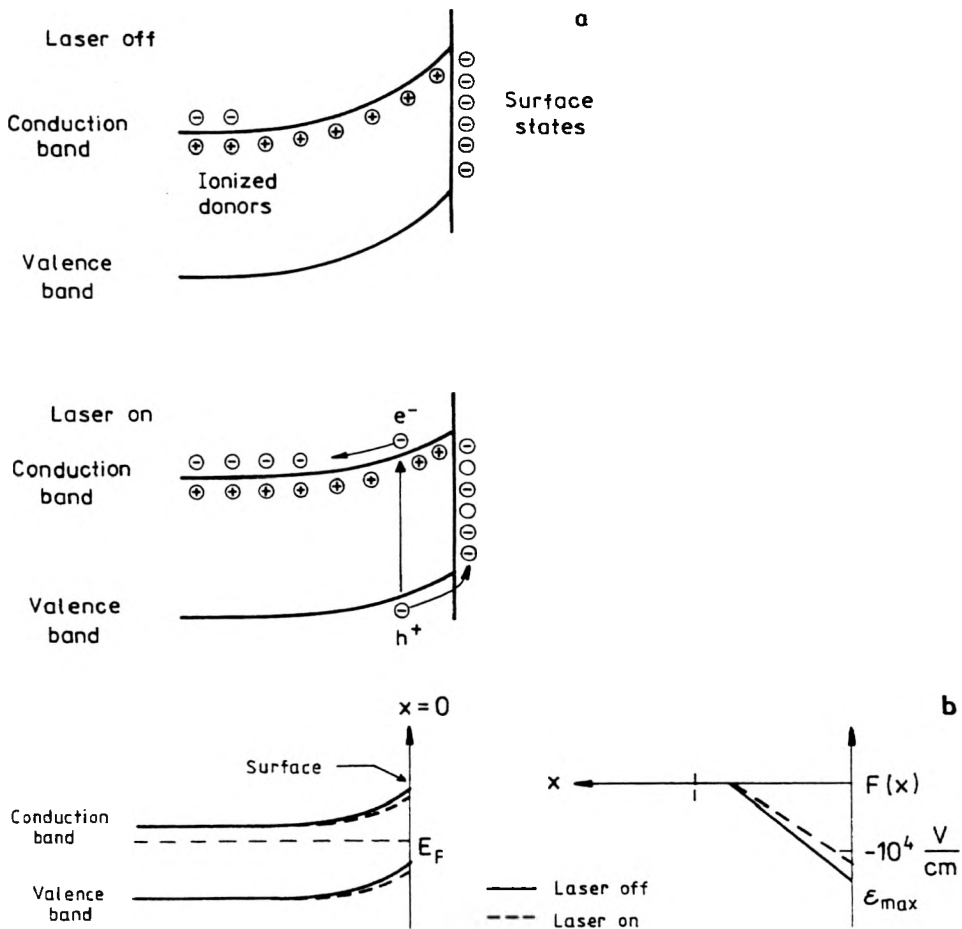
Fig. 3. Schematic representation of the photoreflectance effect (a), and the photoinduced changes in the surface built-in electric field (b), for an n-type semiconductor.

(where ΔR is the change in reflectivity caused by a pump beam). Since it is the quantity $\Delta R/R$ that is of interest, the common factor I_0 is eliminated.

In the case of photoreflectance, it is important for the apparatus to have good filtering of the stray laser light, because it has the same frequency (chopped) as the signal of interest and can be easily detected. The scattered pump light can be reduced by means of an appropriate low-pass filter in front of the detector. Furthermore, laser illumination can produce band gap photoluminescence, which under certain conditions is greater in intensity than the signal of interest. This problem can be eliminated by using long-focal-length optics or by using a second monochromator running in unison with the probe monochromator [9]. For a double mono-chromator, two scans are taken, one with the probe light on and one without it. Subtracting the two traces effectively eliminates the photoluminescence (PL). An alternative technique involves use of a dye laser as the probe beam and a detector placed sufficiently far away from the sample so as to reduce the PL, which is usually emitted isotropically [10], [11]. The spurious photoluminescence background signal can also be reduced or eliminated by using, for example, a double detector system [12], sweeping photoreflectance [13], or double pump beam method called differential photoreflectance [14].

3. Electromodulation

In photoreflectance spectroscopy, the differential changes in the reflectivity coef-ficient are measured. We can define the changes as follows:

$$\frac{\Delta R}{R} = \frac{R_{off} - R_{on}}{R_{off}} \tag{1}$$

where R_{off} and R_{on} are the reflectivity coefficients when the pump beam (laser) is off and on, respectively. These normalised changes can be related to the perturbation of the dielectric function $(\varepsilon = \varepsilon_1 + i\varepsilon_2)$ [15]

$$\frac{\Delta R}{R} = \alpha(\varepsilon_1, \varepsilon_2)\Delta\varepsilon_1 + \beta(\varepsilon_1, \varepsilon_2)\Delta\varepsilon_2 \tag{2}$$

where α and β are the Seraphin coefficients, and $\Delta\varepsilon_1$ and $\Delta\varepsilon_2$ are the changes of the real and imaginary part of ε, respectively, related by Kramers–Kronig inversion. In the vicinity of the fundamental gap of bulk materials $\beta \approx 0$ [16], so that $\Delta R/R \approx \alpha(\varepsilon_1, \varepsilon_2)\Delta\varepsilon_1$ is the only term that is important. However, in multilayer structures interference effects are important so that both $\Delta\varepsilon_1$ and $\Delta\varepsilon_2$ may have to be considered. The functional form of $\Delta\varepsilon_1$ and $\Delta\varepsilon_2$ can be calculated for a given perturbation provided that the dielectric function and critical point are known.

As mentioned above, the photoreflectance spectroscopy is one of the elec-tromodulation techniques and thus we will discuss the line shapes of the PR response in terms of electromodulation mechanisms. Electromodulation is the most complex form of modulation spectroscopy. This perturbation can destroy the translational symmetry of the material and hence can accelerate unbound electrons and/or

holes [16]. It is exactly this aspect of electromodulation that produces a sharp, third derivative line shape under certain electric field conditions. However, for bound states such as excitons, impurities, quantum wells, the perturbing field does not accelerate electrons and/or holes. These types of particles do not have translational symmetry and are confined in space. Their energy spectrum is discrete and not continuous as in the case of unbound particles. In this situation the modulating field can alter the binding energy of the particle (Stark effect). In addition, the field can cause the intensity of the transition to vary through a physical separation of the electrons and holes or it can change the lifetime of the state in the case of a finite potential. In the case of bound states the line shape is the first derivative [17], [18].

We will consider the effect of electromodulation in two regimes depending on the intensity of the electric field. First we define the energy called electrooptic energy (energy gained by a free particle in the electric field F) directly related to the strength of this field

$$(\hbar\Omega)^3 = \frac{q^2\hbar^2F^2}{2\mu} \tag{3}$$

with μ being the reduced interband mass in the direction of the field. We have the case of the low field regime when $\hbar\Omega \leqslant \Gamma$, where Γ is the energetic broadening parameter of the particle state. When this is not true we have the case of the intermediate electric field. Both cases can be considered when the electric field is not too strong, which means that $qFa \ll E_g$, where a is the lattice constant (or an appropriate periodic length in microstructure) and E_g is the band gap. In this situation the band structure is unchanged. If $qFa \approx E_g$, we have the so-called high field regime and the Stark shifts are produced.

3.1. Third derivative spectroscopy

For the case of free carriers in solid, we consider the case of low field modulation from or to flat band. Below, we present a very well-known approach after [17], based on a simple physical derivation of the effects of an electric field on dielectric function. A more rigorous and elegant treatment has been given by ASPNES and ROWE [16], [19]. We begin by calculating the energy gained by a free particle in an electric field. This can be obtained by replacing k by $k + qFt/\hbar$. Following Aspnes and Rowe [16], [19], we find that the energy gained is

$$E(F) = \frac{q^2F^2t^2}{2\mu} \tag{4}$$

where t is the time. If we consider an optical structure near a critical point, with energy E_g, the dielectric function has the general form

$$\varepsilon = \varepsilon(E - E_g, \Gamma) \tag{5}$$

where E is the photon energy.

The electric field induced change in the dielectric function is given by

$$\Delta\varepsilon = \varepsilon(E - E_g + E(F)) - \varepsilon(E - E_g). \tag{6}$$

If the field is sufficiently small (low field regime), Eq. (6) can be expanded in a Taylor series to yield

$$\Delta\varepsilon = E(F)(\mathrm{d}/\mathrm{d}E)\varepsilon(E - E_g, \Gamma) = (q^2 F^2 t^2/2\mu)(\mathrm{d}/\mathrm{d}E)\varepsilon(E - E_g, \Gamma). \tag{7}$$

In quantum mechanics, the time t is also an operator

$$t = i\hbar(\mathrm{d}/\mathrm{d}E), \tag{8}$$

so that Eq. (6) becomes

$$\Delta\varepsilon = (q^2 F^2 \hbar^2/2\mu)(\mathrm{d}^3/\mathrm{d}E^3)\varepsilon(E - E_g, \Gamma) = (\hbar\Omega)^3(\mathrm{d}^3/\mathrm{d}E^3)\varepsilon(E - E_g, \Gamma). \tag{9}$$

Equation (9) has all of the essential features of low field electromodulation. The quantity $\Delta\varepsilon$ is proportional to the quantity F^2, inversely proportional to the reduced mass μ and has a line shape that is the third derivative of the unperturbed optical function. Note also that the condition $E(F) \leqslant \Gamma$ is equivalent to $\hbar\Omega \leqslant \Gamma$, if we take $\tau\Gamma = \hbar$, where τ is a characteristic lifetime.

In order to evaluate Eq. (9) one must know the dielectric function and the critical point type. For the case of homogeneous broadening the dielectric function takes a generalised Lorentzian form. For this dielectric function, the change in reflectivity can, in general, be written as

$$\Delta R/R = \mathrm{Re}\left[e^{i\varphi}(E - E_g + i\Gamma)^{-m}\right] \tag{10}$$

where φ is a phase factor and m depends on the type of the critical point; *e.g.*, for three dimensional M_0 critical point the parameter $m = 2.5$.

3.2. Franz–Keldysh oscillations

In the event that the low field criterion is not satisfied, but still there is $qFa \ll E_g$, the dielectric function can exhibit Franz−Keldysh oscillations (FKO). We shall give a simple physical picture of this phenomenon [3]. It will be assumed here that the broadening paremeter $\Gamma = 0$.

Under the influence of an electric field F in the z-direction the energy bands are tilted by an amount qFz. An electron attempting to tunnel from the valence band into the conduction band sees a triangular barrier. If during the tunneling process the electron interacts with a photon of energy E, the effective width of the barrier to be transferred has to be made smaller. In general, the probability of transmission T through the barrier is given by

$$T = \exp(-2\int k\,\mathrm{d}z) \tag{11}$$

where the integral is between the classical turning points and

$$\frac{\hbar k^2}{2\mu} = E_g - E - qFz. \tag{12}$$

The integral yields

$$T = \exp\left(-\frac{4}{3}\eta^{3/2}\right) \tag{13}$$

where

$$\eta = \frac{E_g - E}{\hbar\Omega}. \tag{14}$$

Equation (13) contains most of the essential features of FKO. For $\eta > 0$ ($E < E_g$), the transmission probability is exponential as a consequence of the photon-assisted tunneling. However, for $\eta < 0$ ($E - E_g$), the transmission probability becomes an oscillatory function.

In a more rigorous treatment, it can be shown that for a three dimensional critical point the dielectric function in the presence of the field F (neglecting Γ) can be written as [2], [5]

$$\varepsilon(E - E_g, F) = 1 + \left[\frac{C(\hbar\Omega)^{1/2}}{E^2}\right][G(\eta) + F(\eta)] + \frac{D(2\sqrt{E_g} - \sqrt{E_g + E})}{E^2} \tag{15}$$

where

$$G(\eta) = \pi[Ai'(\eta)Bi'(\eta) - \eta Ai(\eta)Bi(\eta) + (-\eta)^{1/2}H(-\eta)], \tag{16}$$

$$F(\eta) = \pi[Ai'^2(\eta) - \eta Ai'^2(\eta) - (-\eta)^{1/2}H(-\eta)]. \tag{17}$$

The quantities $G(\eta)$ and $F(\eta)$ are referred to as electrooptic functions, while $Ai(\eta)$, $Ai'(\eta)$ and $Bi(\eta)$ and $Bi'(\eta)$ are Airy functions and their derivatives, and $H(-\eta)$ is the unit step function. The parameters C and D are related to matrix element effects and can be considered constant in the vicinity of the critical point.

For the case of an M_0 critical point we can write

$$\Delta\varepsilon_2(\eta) = \varepsilon_2(E - E_g, F) - \varepsilon_2(E - E_g, 0) = \left[\frac{C(\hbar\Omega)^{1/2}}{E^2}\right]F(\eta). \tag{18}$$

In Figure 4, the imaginary parts of Eqs. (15) and (18) are plotted. The curve in Fig. 4b looks qualitatively similar to that described by Eq. (13), *i.e.*, an exponential tail for $\eta > 0$ and an oscillatory function for $\eta < 0$. From Eqs. (13) and (18) the positions of the n-th extrema in the FKO are given by

$$n\pi = \frac{4}{3}\left(\frac{E_n - E_g}{\hbar\Omega}\right)^{3/2} + \theta \tag{19}$$

where E_n is the photon energy of the n-th extrema and θ is an arbitrary phase factor. A plot of $\frac{4}{3\pi}(E_n - E_g)^{3/2}$ versus the index number n will yield a straight line with slope $(\hbar\Omega)^{3/2}$. Therefore, the electric field F can be directly obtained from the period of FKO if the value of μ is known. Conversely, μ can be measured if the field is known.

The period of the FKO is determined by the dominant field in the structure. In the above expressions the nature of that field has not been specified. There are
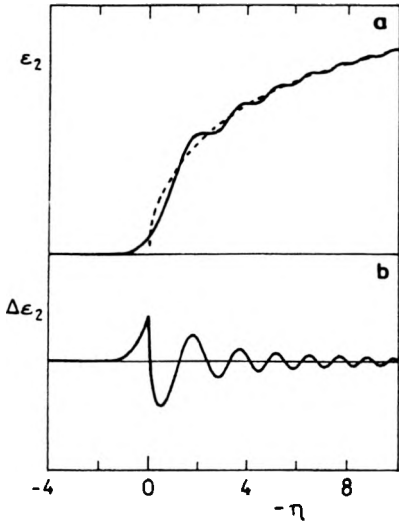
Fig. 4. Imaginary part of Eq. (15) — solid line, and $\varepsilon_2(E-E_g, 0)$ — dotted line (a); dependence $\Delta\varepsilon_2$ according to Eq. (18) (b), [3]

two limiting cases to be considered. If modulation is from flat band, *i.e.*, no presence of DC field, then the field is clearly the modulating field F_{AC}. A more interesting situation occurs when there exists a large DC electric field in the material and a small modulating field is applied, *i.e.*, $F_{AC} \ll F_{DC}$. In this case the period of the FKO is given by F_{DC} and not F_{AC} [20]. SHENand and POLLAK [20] have even considered the case when F_{AC} is not small compared to F_{DC}. They have shown that even for F_{AC}/F_{DC} as large as 0.15 the few FKO's are still determined by F_{DC}.

4. Properties of semiconductor bulk and epilayers

In this section, we will discuss the use of the photoreflectance spectroscopy to study the bulk properties of semiconductors, such as the composition of multinary semiconducting compounds, carrier concentration, characteristic lifetimes of carriers, distribution of the built-in electric field, the influence of perturbations such as temperature, strain and effects of growth and processing. While a number of studies devoted to these problems have actually been performed on epitaxial (or thin) layers, they appear not to explicitly depend on the geometry of the films but rather on their bulk properties. In Sect. 4.3 and 4.7 we will discuss the explicit studies of layered homo- and heterostructures.

4.1. Composition of alloys

One of the extremely important parameters of a semiconductor is the composition of binary A_xB_{1-x}, ternary $A_xB_{1-x}C$ or quaternary $A_xB_{1-x}C_yD_{1-y}$ alloys. The compositional variation of the fundamental transition E_0 and/or higher lying features E_1 has been investigated by photoreflectance for a large number of alloys, including $Cd_xMn_{1-x}Te$ (for $x \leqslant 0.6$) at room and liquid helium temperatures [21], $Al_xIn_{1-x}P$
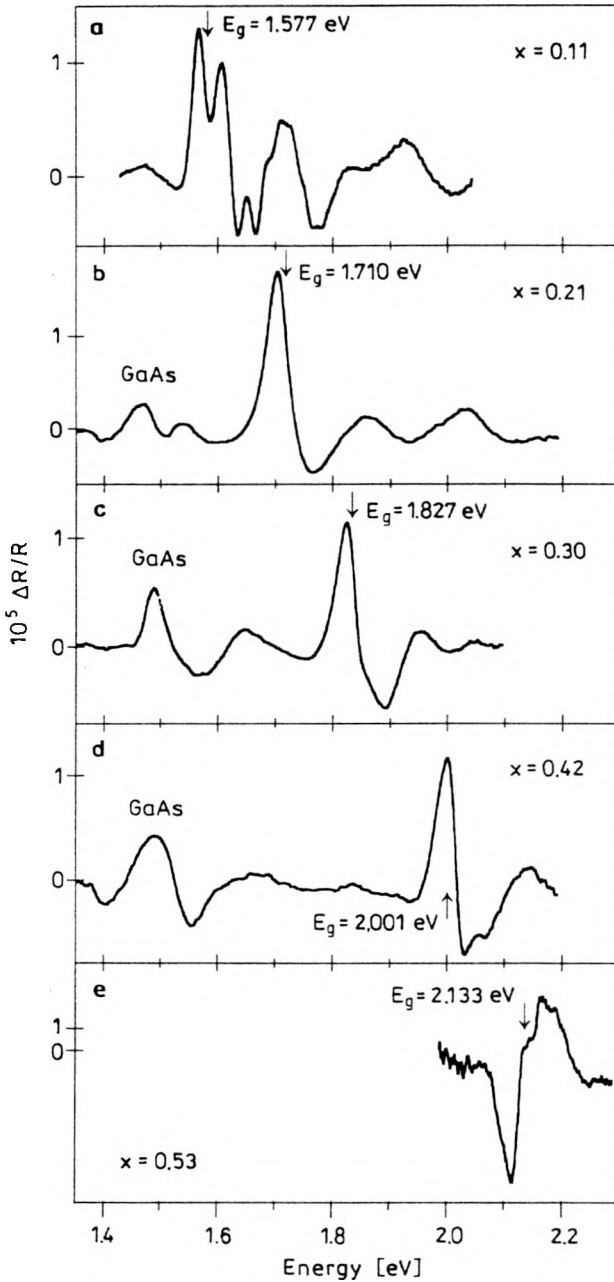
Fig. 5. Room temperature PR spectra of $Al_xGa_{1-x}As/GaAs$ structures as a function of aluminium content x [27]. Arrows mark the band gap energies of $Al_xGa_{1-x}As$.

[22], $CuAl_xGa_{1-x}Se_2$ [23], $CuAl(S_xSe_{1-x})_2$ [24], $In_xGa_{1-x}N$ [25], $Al_xGa_{1-x}As$ (for $x \leqslant 0.45$) [26] and $Al_xGa_{1-x}As$ (for $x \leqslant 0.6$) [27]. In Figure 5, the PR spectra obtained by SITAREK et al. [26] of several $Al_xGa_{1-x}As$ layers grown by MBE

(molecular beam epitaxy) on GaAs substrates are shown versus aluminium content. The spectra are quite complicated because the Franz–Keldysh oscillations are observed and also the signal related to the GaAs buffer is seen. On the basis of the transition energies derived from the spectra the dependence of the E_0 ($Al_xGa_{1-x}As$) on the composition of alloy has been determined as

$$E_0(x) = (1.430 \pm 0.004) + (1.34 \pm 0.02)x. \qquad (20)$$

This relation has been compared with the results from the literature [28] as presented in Fig. 6.
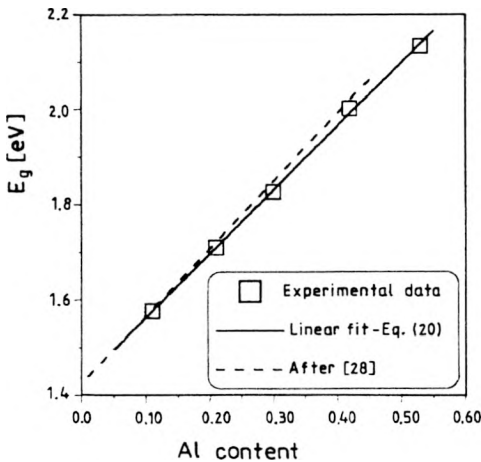
Fig. 6. Band gap energy of $Al_xGa_{1-x}As$/GaAs versus aluminium content from PR experiment (squares), see Fig. 5. Solid line — linear approximation to the experimental data; dashed line — taken after [28].

4.2. Carrier concentration

There are a number of reports on the use of photoreflectance in investigations of carrier concentration and mainly the effects of changes in concentration of dopants resulting in changes of carrier concentration. PETERS *et al.* [29] have used the photoreflectance spectroscopy as a method for calibration of the *n*-type doping in Si-doped GaAs. They have studied the blue shift of the fundamental band gap of GaAs with an increase of the doping concentration. They have found a linear correlation between the concentration of dopants and the value of the energy gap shift. They have based their explanation for this effect on some competition between the many body effects and Burstein–Moss effect related to the filling of the conduction band. Such an effect has also been observed in *n*-type [30] and *p*-type [31] GaAs. LEE *et al.* [30] have extended the results of PETERS *et al.* [29] for Si-doped samples for concentrations from 1×10^{17} cm^{-3} up to almost 1×10^{19} cm^{-3}.

Similar effects have been investigated by PR for the MOCVD (metal-organic chemical vapour deposition)-grown Si-doped GaN layers. This time, a linear dependence between the fundamental gap transition energy and the cubic root

of carrier concentration has been found [32]. This red shift of the band gap with the increase of the level of Si doping has been fully explained by the many body effects (the renormalisation of the band gap).
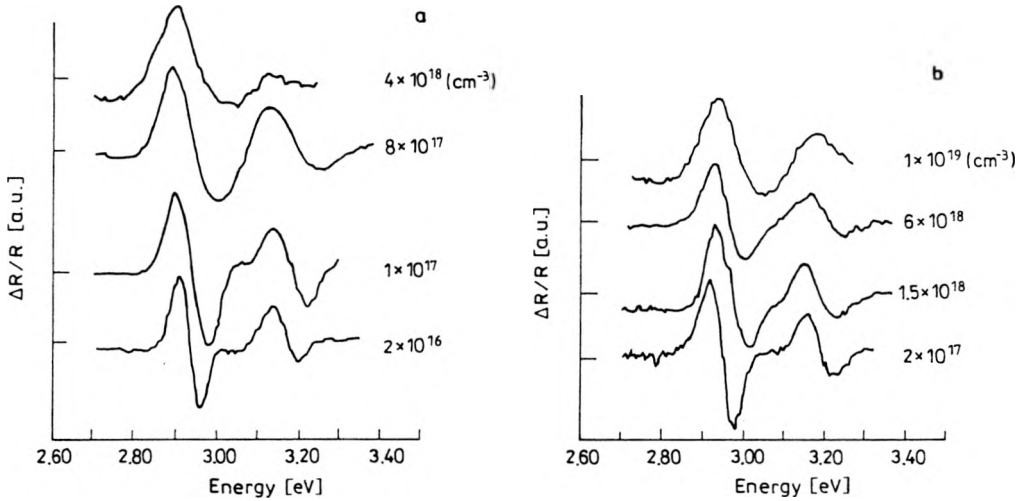

Fig. 7. PR response of GaAs as a function of carrier concentration: **a** — for Si:GaAs, **b** — for Zn:GaAs [33].
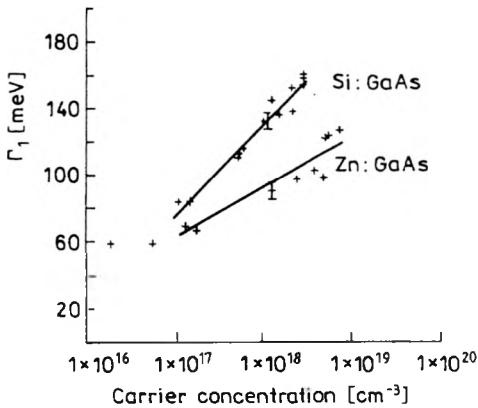

Fig. 8. PR broadening parameter as a function of carrier concentration [33].

The effects of carrier concentration can be studied in photoreflectance not only at the fundamental band gap. BADAKHSHAN *et al.* [33] have investigated the PR spectra of MOCVD-grown Si:GaAs (*n*-type) and Zn:GaAs (*p*-type) layers at the energy of E_1 and $E_1 + \Delta$ transitions. They have observed almost no shift in energy of those transitions but very strong increase of broadening parameter Γ_1 with the increase of carrier concentration. In Figure 7, the PR spectra as a function of doping concentration and doping type are shown. In Figure 8, the linear dependence of broadening versus logarithm of carrier concentration is presented.

4.3. Layer thickness

If it is not really the bulk material, that is under investigation but thin (epitaxial) semiconductor layer, it is possible to observe oscillations in PR spectra for energies below the fundamental gap of semiconductor. These effects are associated with the interference of light beams reflected from different interfaces. The observation of those spectral features can be used to evaluation of the epilayer thickness. This kind of oscillation in photoreflectance has been observed in many cases, including GaAs on GaAs homolayers [34], [35], GaAs/Al$_x$Ga$_{1-x}$As [36] and for CdTe/Si [37] heterostructures.

In order to explain this problem in a simple way, we have to take the system containing two interfaces only: air/film and film/substrate [34]. A schematic diagram of the interfaces and the notation used is shown in Fig. 9. In general, the measured quantity in PR experiments is $\Delta R/R$ versus wavelength. The dependence $\Delta R/R$ at a wavelength λ can be expressed as

$$\Delta R/R = (R'/R) - 1 \tag{21}$$

where R' and R are the modulated (laser on) and unmodulated (laser off) reflectances, respectively. It follows that $R' = f(\lambda, n_f + \delta n_f, n_s + \delta n_s, d_f)$ and $R = f(\lambda, n_f, n_s, d_f)$, where n_f and n_s are the refractive indices of the film and substrate, respectively, δn_f and δn_s are their respective changes due to modulation, and d_f is the thickness of the epilayer.

In general, the reflected intensity (reflectance) for unpolarized light can be given by

$$R = \frac{1}{2}(r^p r^{p*} + r^s r^{s*}) \tag{22}$$

where r^p and r^s, associated with the p- and s-polarizations states, are given by
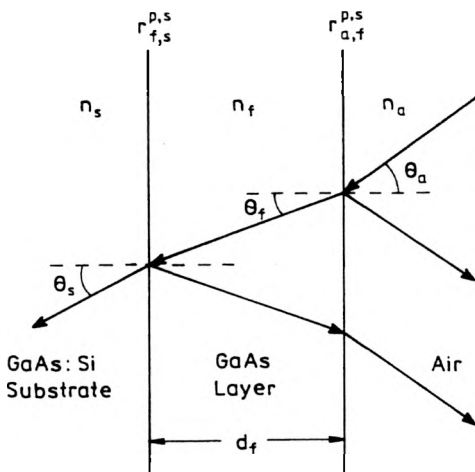
Fig. 9. Schematic diagram of the two-interface model used for calculation of the $\Delta R/R$ in the multilayer sample.

$$r^{p,s} = (r^{p,s}_{a,f} + r^{p,s}_{f,s} e^{-ix}).$$ (23)

In Equation (23), for a film thickness d_f

$$x = (2\pi/\lambda)2n_f d_f \cos\theta_f,$$ (24)

and $r_{a,f}$ or $r_{f,s}$ are the reflection copefficients for p- and s-polarized radiation appropriate to the air/film and the film/substrate interfaces, respectively. The reflected amplitudes (reflectivity) from the air/film interface are given by

$$r^p_{a,f} = [\tan(\theta_a - \theta_f)]/[\tan(\theta_a + \theta_f)],$$ (25)

$$r^s_{a,f} = -[\sin(\theta_a - \theta_f)/[\sin(\theta_a + \theta_f)]$$ (26)

and similar relations can be written for the film/substrate interface for the two polarizations. Well below the fundamental gap of undoped semiconductor, where the oscillations are observed, the refractive index of the film is not modulated, so $\delta n_f \approx 0$ and only $\delta n_s \neq 0$. The latter is a function of wavelength and, assuming normal incidence, it is expressed from $R_s = (n_s - 1)^2/(n_s + 1)^2$ as

$$\delta n_s = \frac{1}{4}(n_s^2 - 1)(\Delta R_s/R_s),$$ (27)

$\Delta R_s/R_s$ for the substrate in Eq. (27) has been expressed as an exponential function of energy using the envelope of the interference oscillations observed in PR spectra. KALLERGI et al. [34] have used Eqs. (22)−(27) to generate the PR spectra of GaAs/GaAs samples in the range below the energy of band gap, and from the best fit to the experimental data they have obtained the thickness of the epilayer. In Fig. 10, the computer generated and measured spectra for two GaAs epilayers are compared. The thicknesses obtained are in good agreement with the results of SEM (scanning electron microscopy) measurements.

4.4. Trap states

It has been demonstrated that the frequency dependence of the PR signal can be used to evaluate the states lying deeply in energy gap, called trap levels, due to the modulation of the electric field through a recombination of minority speciel with charge in traps [38]−[42]. Thus PR can be closely related to capacitance-voltage techniques such as DLTS (deep level transient spectroscopy).

It has been observed that the magnitude $\Delta R/R$ of the photoreflectance signal decreases with increasing modulation frequency f_m. This dependence can be accounted for on the basis of the following considerations [40]. The chopped pump radiation can be considered as a square wave source. When light impinges on the sample, electron–hole pairs are created. These charges are then free to fill traps and modify the electric field strength. We assume that these excess carriers abruptly change the built-in electric field. Typically the response time in such processes is less than 100 µs [43]. When the light is switched off, the trap population and the electric field strength decay with a characteristic time τ, causing a restoration of the original potential. Thus, for the chopping frequency f_m it can be shown that the Fourier
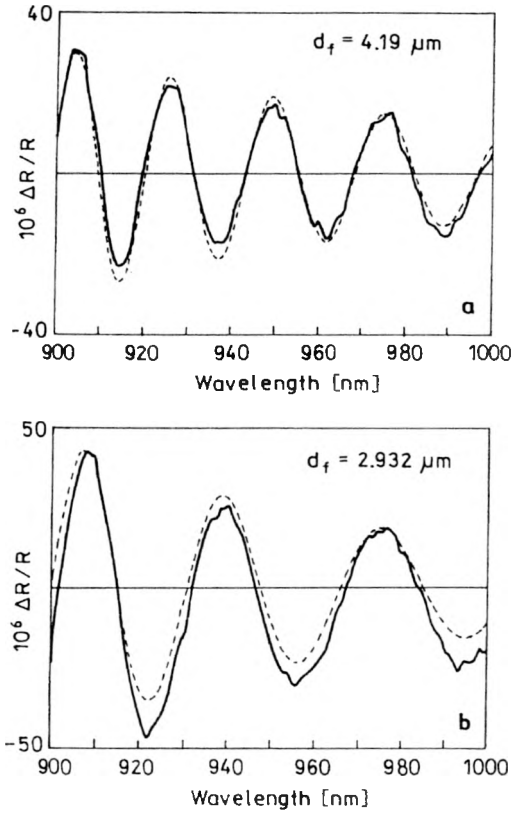
Fig. 10. Experimental (solid line) and theoretical (dashed line) PR spectra of two GaAs samples with different epilayer thickness [34].

component of the PR intensity $\Delta R(f_m)/R$ is given by

$$\frac{\Delta R(f_m)}{R} = \sum_{i=1}^{n} \left(\frac{\Delta R(0)}{R}\right)_i A(f_m \tau_i) \tag{28}$$

where

$$A^2(f_m, \tau_i) = \frac{4 + f_m^2 \tau_i^2 \left[1 - \exp(-\pi/f_m \tau_i)\right]^2}{4(1 + f_m^2 \tau_i^2)}, \tag{29}$$

τ_i is the characteristic time constant of the i-th trap state and $[\Delta R(0)/R]_i$ is the PR signal produced by the modulation of the i-th trap state in the limit of $f_m \rightarrow 0$.

In Figure 11, we have plotted the amplitude of the PR signal as a function of modulation frequency for semi-insulating GaAs for several values of temperature [40]. It has been assumed for these experimental data that in this ferquency range $n = 2$ and $[\Delta R(0)/R]_2 A(f_m \tau_2) \ll [\Delta R(0)/R]_1 A(f_m \tau_1)$, with $\tau_1 > \tau_2$. Plotted by the solid lines in Fig. 11 are the least-squares fits of Eqs. (28), (29) to the experimental data. From this analysis it is possible to evaluate $\tau_i(T)$ in measured temperature range.
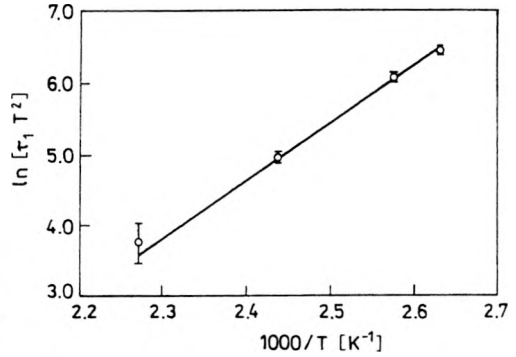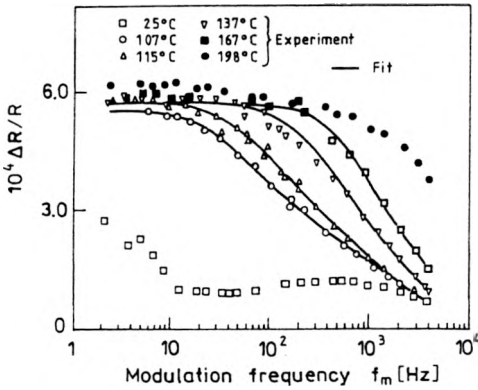
Fig. 11. Amplitude of PR signal of semi-insulating GaAs as a function of chopping frequency f_m for several temperatures [40].

Fig. 12. Plot of $\ln(\tau_1 T^2)$ as a function of $1000/T$ [40]. The solid line is a least-squares fit to a linear function.

In Figure 12, $\ln(\tau_1 T^2)$ is plotted as a function of $1000/T^2$. The solid line is a least-squares fit to a linear function yielding in activation energy $\Delta E = 0.70 \pm 0.05$ eV. Such an activation energy corresponds to two different types of trap states that may occur in a GaAs, *i.e.*, surface states (responsible for Fermi level pinning) or EL2.
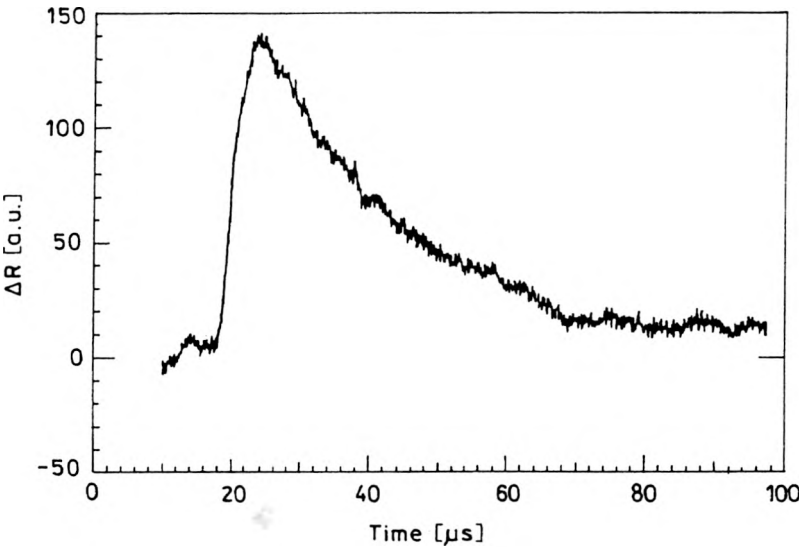
Fig. 13. Time resolved ΔR signal of $Al_{0.057}Ga_{0.953}As$ [53].

Information about trap states can also come from direct studies of the time constants involved in PR experiment. There are also many resports concerning the

direct investigations of time decay (rise and fall times) of the photoreflectance signal to determine the characteristic time constants of states involved in the modulation process. Most of those works have concerned the investigation of GaAs [44] − [51]. Other materials have also been investigated, including $In_{0.5}Ga_{0.5}P_{0.99}As_{0.01}$ [52] and $Al_{0.057}Ga_{0.943}As$ [53]. In Figure 13, an example of time dependence of PR signal at the energy of the fundamental band gap of the $Al_{0.057}Ga_{0.943}As$ is shown. The decay time has been found to be 22 μs, which corresponds to the capture of electrons by surface states. SHEN *et al.* [44] have concluded that since the rise and fall times are approximately equal, the dynamics of the PR are not related to a trap state but are due to majority carrier flow.

4.5. Temperature dependence

The temperature dependence of energy and broadening parameter of the band gap of semiconductor can be the source of different information about the scattering effects. The two most popular relations describing the temperature dependence of band gap are:

— the semiempirical Varshni expression

$$E_0(T) = E_0(0) - \frac{\alpha T^2}{\beta + T}, \tag{30}$$

— the Bose–Einstein expression [54], [55]

$$E_0(T) = E_0(0) - \frac{2a_B}{\exp(E_{ap}/kT) - 1} \tag{31}$$

where a_B represents the strength of the electron–phonon interaction and E_{ap} corresponds to an average phonon energy. The temperature shift E_0 contains contributions from both thermal expansion and electron–phonon coupling effects. Therefore, in order to obtain parameters directly related to the latter influence, it is necessary to eliminate the contribution of the former. For example, the quantities α and β of Eq. (30) and a_B and E_{ap} of Eq. (31) include the influence of the lattice dilation. The energy shift ΔE_{th} due to the termal expansion can be written as

$$\Delta E_{th} = -3a\alpha_{th}T \tag{32}$$

where a is the hydrostatic deformation potential and α_{th} is the linear expansion coefficient. Equations (30) and (31) can be written as:

$$E_0(T) - \Delta E_{th} = E_0(0) - \frac{\alpha' T^2}{\beta' + T}, \tag{33}$$

$$E_0(T) - \Delta E_{th} = E_0(0) - \frac{2a'_B}{\exp(E'_{ap}/kT) - 1}. \tag{34}$$

MANOOGIAN and WOOLEY [56] have suggested that after removing the thermal expansion term the paremeter β' of Eq. (33) is directly proportional to the Debye temperaturee Θ_D by the relation $\beta' = 3/8\Theta_D$.

The parameter α' of Equation (33) can be related to a'_B and E'_{ap} of Equation (34) by taking the high-temperature limit of both expressions, yielding $2\hbar a'_B/E'_{ap}$.

The variation of the linewidth (broadening parameter) with temperature can also be expressed by a Bose–Einstein type expression [54], [55]

$$\Gamma(T) = \Gamma(0) + \frac{\Gamma_{ep}}{\exp(E_p/kT) - 1}. \tag{35}$$

The first term of this equation corresponds to broadening mechanisms due to intrinsic lifetime, electron–electron interaction, impurity, dislocation and alloy scattering effects. The paremeter Γ_{ep} is an electron–phonon coupling constant and E_p is the relevant phonon energy. For the direct gap of semiconductors the appropriate phonon energy is the zone-center LO phonon, i.e., $E_p = E_{LO}$ and Γ_{ep} is the electron–LO phonon coupling constant [54], [55].

Photoreflectance spectroscopy has been used to measure the temperature variation of the energy gap of GaAs [40], [57], InP [58], $Al_{0.18}Ga_{0.82}As$ [40], [59], $In_xGa_{1-x}As$ on GaAs for various values of x [60]–[63], $In_{0.53}Ga_{0.47}As$ on InP (also for the $E_0 + \Delta_0$ transition) [64], $In_{0.515}Ga_{0.485}As$ on InP [65], [66], CdTe [67], $Cd_{0.72}Mn_{0.28}Te$ [68], $Cd_{0.9}Mn_{0.1}Te$ [21], InAs [69], wurtzite GaN [70].
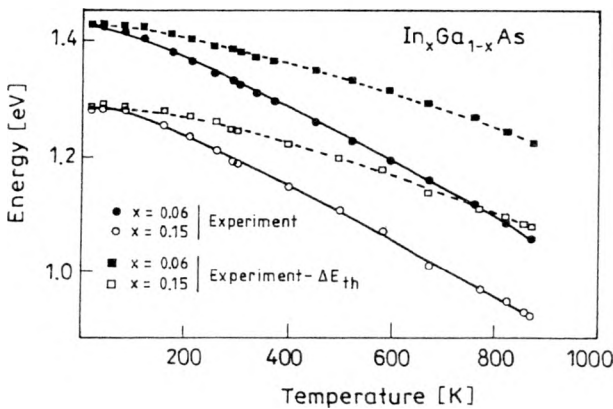
Fig. 14. Experimental temperature dependence of E_g of $In_xGa_{1-x}As$ for $x = 0.06$ (closed circles) and $x = 0.15$ (open circles) [60]. The closed and open squares are the data minus the thermal expansion contribution ΔE_{th}, for $x = 0.06$ and $x = 0.15$ samples, respectively. The solid and dashed lines are least-squares fits to Eqs. (30) and (33).

In Figure 14, the experimental temperature dependence of the direct gap of $In_{0.06}Ga_{0.94}As$ and $In_{0.15}Ga_{0.85}As$ is presented [60]. The solid lines are least-squares fits to the Varshni and Bose–Einstein relationships defiend by Eqs. (30) and (31), and the dashed lines are the fits according to Eqs. (33) and (34). The obtained values of $E_0(0)$, α, β and α', β' as well as a_B, E_{ap} and a'_B, E'_{ap} for both samples are listed in Tabs. 1 and 2, respectively. The values α, β and a_B, E_{ap} for the $In_xGa_{1-x}As$ are found to be similar to those of GaAs [54], [71] because of the low In concentration of those layers.

T a b l e 1. The values of the fitting parameters according to Eqs. (30) and (33) for $In_{0.06}Ga_{0.94}As$ and $In_{0.15}Ga_{0.85}As$ layers [60]. For comparison, the respective parameters for GaAs are also shown.

Material	$E_0(0)$ [eV]	α [10^{-4} eV/K]	β [K]	α' [10^{-4} eV/K]	β' [K]
$In_{0.06}Ga_{0.94}As$	1.420 ± 0.005	4.8 ± 0.4	200 ± 50	2.5 ± 0.4	140 ± 40
$In_{0.15}Ga_{0.85}As$	1.285 ± 0.005	5.0 ± 0.4	231 ± 40	2.6 ± 0.4	150 ± 40
GaAs	1.512 ± 0.005	5.1 ± 0.5	190 ± 82		

T a b l e 2. The values of the fitting parameters according to Eqs. (31) and (34) for $In_{0.06}Ga_{0.94}As$ and $In_{0.15}Ga_{0.85}As$ layers [60]. For comparison, the respective parameters for GaAs are also shown.

Material	$E_0(0)$ [eV]	a_B [meV]	E_{ap} [eV]	a'_B [meV]	E'_{ap} [eV]
$In_{0.06}Ga_{0.94}As$	1.422 ± 0.014	44 ± 9	17.5 ± 3.9	33 ± 7	24.1 ± 3.9
$In_{0.15}Ga_{0.85}As$	1.286 ± 0.015	53 ± 10	20.5 ± 4.4	39 ± 8	25.9 ± 4.4
GaAs	1.514 ± 0.023	57 ± 29	20.7 ± 8.8		

In Figure 15, the temperature dependence of $\Gamma(T)$ for the same $In_x Ga_{1-x}As$ layers is displayed [60]. The solid lines are the least-squares fits to Eq. (35). The obtained values of $\Gamma_0(T)$, Γ_{ep} and E_p are given in Tab. 3. HANG *et al.* [60] have found that $E_p = E_{LO}$, where E_{LO} for the $In_x Ga_{1-x}As$ has been evaluated from the Raman scattering. Due to the low In composition of the material E_{LO} for the $In_x Ga_{1-x}As$ is close to the GaAs value. Also, it has been found that Γ_{ep} for both samples is similar to that for direct gap of GaAs [72]. The difference in $\Gamma_0(0)$ has been explained in terms of material quality.

It is interesting to note that the phonon energy E_p entering into the temperature dependence of $\Gamma(T)$ is generally found to be greater than E'_{ap}, which is appropriate for $E(T)$. For the $In_x Ga_{1-x}As$ materials these quantities are 33 meV and 25 meV. The reason for the difference is that E'_{ap} represents an average energy for both optic and acoustic phonons while E_p is the LO phonon energy.
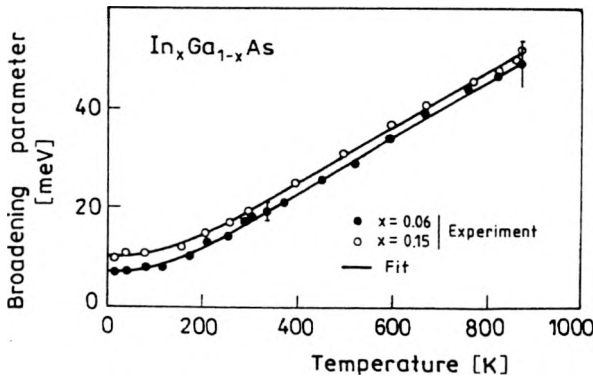

Fig. 15. Temperature variation of the broadening parameter of E_g of $In_x Ga_{1-x}As$ for $x = 0.06$ (closed circles) and 0.15 (open circles) [60]. The solid lines are least-squares fits to Eq. (35).

T a b l e 3. The values of the fitting parameters according to Eq. (35) for $In_{0.06}Ga_{0.94}As$ and $In_{0.15}Ga_{0.85}As$ layers [60].

Material	$\Gamma(0)$ [meV]	$\Gamma_{ep}(0)$ [meV]	E_p [meV]
$In_{0.06}Ga_{0.94}As$	7.5 ± 0.5	23 ± 6	32 ± 11
$In_{0.15}Ga_{0.85}As$	10.5 ± 0.5	23 ± 6	33 ± 10

4.6. Influence of strain

One of the main goals of strained-layer epitaxy is to create metastable thin films with properties different from those of the corresponding bulk material. Typically, such films are pseudomorphic compound semiconductor structures grown from lattice-mismatch materials by MBE or by MOCVD. Such structures offer nearly complete flexibility in tailoring their electronic and optical properties and have proven to be highly successful in novel microelectronic and optoelectronic devices. This flexibility in tailoring the properties of these devices is enhanced by the possibility of pseudomorphic growth where the lattice mismatch between epilayer and substrate is accommodated by elastic strain. In fact, the in-plane biaxial strain, arising at the interface with the substrate, considerably affects the electronic structure and the optical response of the epilayer. It reduces or increases the band gaps, depending on the sign of the strain. It reduces or removes the interband or intraband degeneracies (*e.g.*, between the heavy and light hole valence bands at $k = 0$). It reduces coupling between neighbouring bands.

Concerning the E_0 optical transitions at $k = 0$, the hydrostatic component of the strain shifts the energy gap between the valence bands and the lowest lying conduction band. In addition, the uniaxial strain component splits the heavy (HH) and light (LH) hole valence bands. The resulting energy gaps between the conduction and the split valence bands are:

$$E_0^{HH} = E_0 + \delta E_H - \frac{\delta E_S}{2}, \tag{36}$$

$$E_0^{LH} = E_0 + \delta E_H + \frac{\delta E_S}{2} - \frac{(\delta E_S)^2}{2\Delta_0} \tag{37}$$

where:

$$\delta E_H = 2a\frac{C_{11} - C_{12}}{C_{11}}\varepsilon, \tag{38}$$

$$\delta E_S = 2b\frac{C_{11} + 2C_{12}}{C_{11}}\varepsilon, \tag{39}$$

while C_{ij} are the elastic stiffness constants, a and b are the hydrostatic and shear deformation potentials, respectively, and ε is the in-plane strain which is given by $\varepsilon = \dfrac{a_S - a_L}{a_L}$, where a_S and a_L are the lattice parameters of the substrate and layer,

respectively. The valence band splitting, as measured from the optical spectra is

$$\Delta E_{\text{split}} = \delta E_S = 2b\,\frac{C_{11}+2C_{12}}{C_{11}}\,\varepsilon. \tag{40}$$

In Figure 16, the PR spectra are presented, showing the heavy and light hole splitting generated by strain in GaAs layers deposited on Si substrates [73]. The quantity ΔE means the splitting between light (feature A) and heavy (feature B) hole bands. The value of the splitting increases with the decrease of the temperature. It has been explained on the basis of the difference in the thermal expansion coefficients of GaAs and Si. From the value of the splitting energy expressed by Eq. (40) the value of the in-plane strain has been estimated to be 0.12%, which has been in agreement with the X-ray diffraction results.
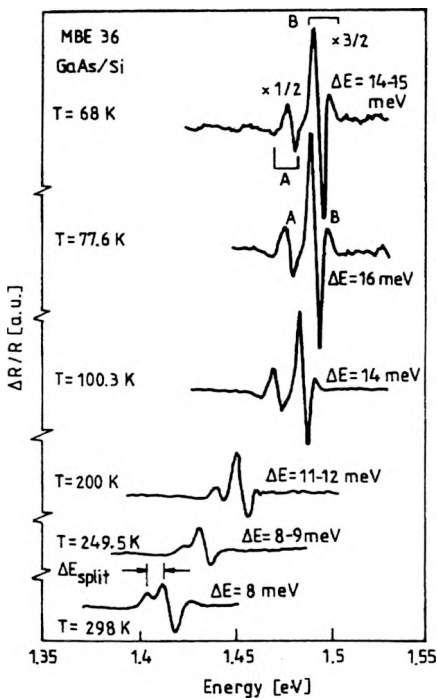
Fig. 16. The PR spectra of strained GaAs on Si at several temperatures [73]. A and B are the light and heavy hole transitions, respectively.

The required strain-dependent properties can be achieved only by carefully controlling the composition and the epilayer thickness, which should be thinner than a critical value d_c to avoid relaxation via misfit dislocations, which drastically lower the layer quality and hence, also the device performance. This problem has also been investigated by photoreflectance spectroscopy for the case of $In_xGa_{1-x}As$ layers grown by MOCVD on GaAs substrates [74], [75]. They have determined the broadening parameter and the PR amplitude of the band gap feature of the
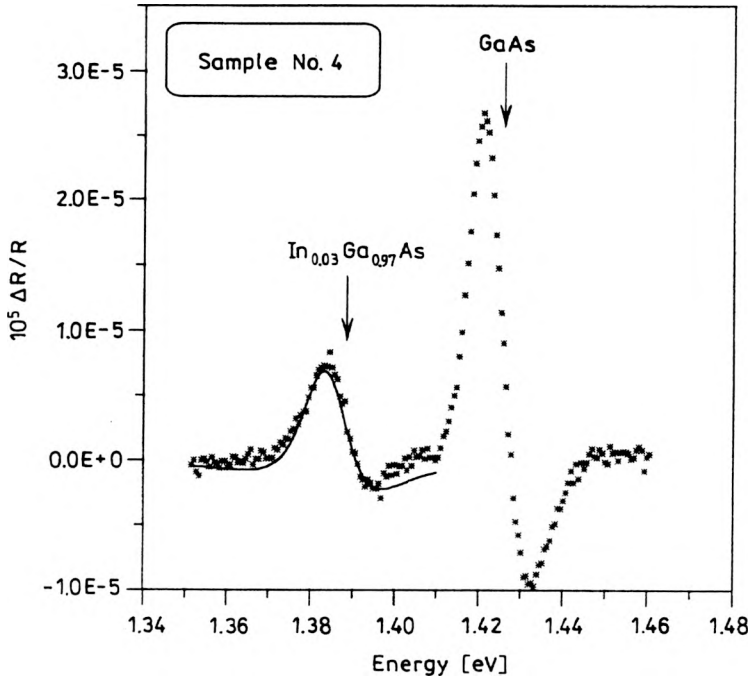
Fig. 17. Room temperature PR spectrum of 100 nm thick strained $In_{0.03}Ga_{0.97}As$ layer on GaAs substrate [75].

$In_xGa_{1-x}As$ for several samples with various indium content and epilayer thickness. An example of the spectrum is shown in Fig. 17. The dependence of the broadening parameter and PR amplitude versus Δd are shown in Figs. 18 and 19. The quantity Δd is defined as the difference between the nominal layer thickness (determined
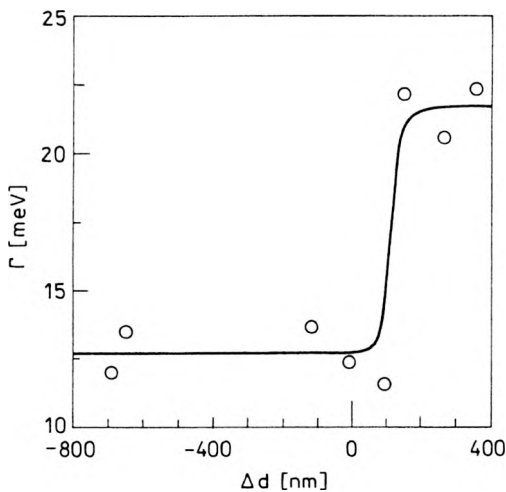

Fig. 18. Broadening parameter of PR signal of several $In_xGa_{1-x}As$ layers on GaAs versus Δd [[75].
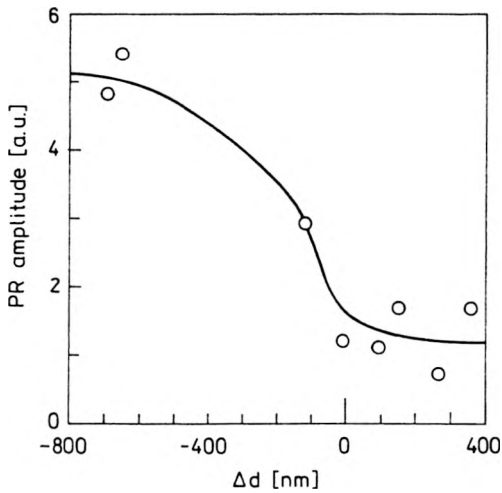
Fig. 19. The PR amplitude of several $In_xGa_{1-x}As$ layers on GaAs versus Δd [75].

from the growth conditions and X-ray diffraction measurements) and its critical value (taken from the theoretical dependence of the critical thickness versus indium content of $In_xGa_{1-x}As$ on GaAs [76]). A very drastic increase of the broadening and decrease of amplitude of the PR signal is observed at $\Delta d = 0$, which corresponds to the overcoming of the critical thickness and the strong degradation of the layer optical properties.

There is a number of works on the PR investigations of strain effects in different material systems, including: $In_xGa_{1-x}As/GaAs$ [77], $In_xGa_{1-x}As/InP$ [66], $In_xGa_{1-x}As/Al_{0.28}Ga_{0.72}As$ [78], InP/Si [79], ZnTe/GaAs [80], CdTe/GaAs [81], GaN on different substrates [82]–[85].

TCHOUNKEU *et al.* [83] have investigated the residual strain effects and the exciton binding energies of GaN epilayers grown by MOCVD on (0001)-oriented sapphire. A comparison of photoluminescence, common reflectivity and photoreflectance spectra for GaAs on sapphire is drawn in Fig. 20 [83]. It is seen that PR allows, in contrast to reflectivity and PL, the observation of all existing excitonic transitions including their excited states.

QIANG *et al.* [86] have used PR at 300 K to investigate the effects of compressive external stress along [001] and [110] on the E_0 and $E_0 + \Delta_0$ transitions in GaAs and $Al_{0.28}Ga_{0.72}As$. From the stress-induced shifts and splittings they have evaluated the hydrostatic and shear deformation potentials of these energy gaps.

4.7. Surface and interface electric field

It has already been discussed in Sec. 3.2 that the observation of the Franz–Keldysh oscillation in photoreflectance spectra allows determination of the built-in electric field in the sample. If the sample consists of one or more epilayers on the substrate, the superposition of two or more PR signals from different depths of the structure is possible. It is possible to have different values of the internal electric field at the
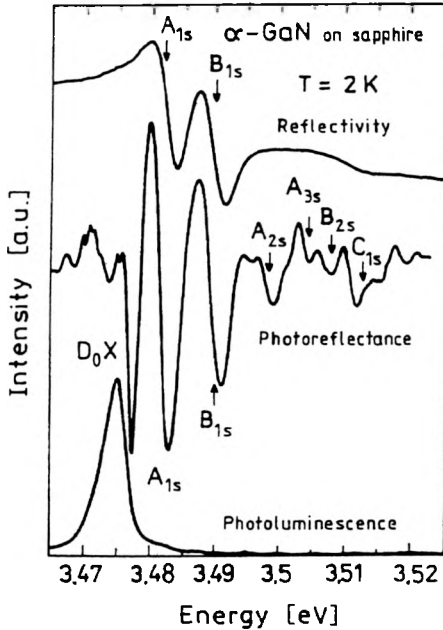
Fig. 20. Comparison of reflectivity, photoluminescence and photoreflectance at 2 K, for GaN layer grown on sapphire [83].

surface or at the particular interface because of the difference in the density of surface and interface states. If we can extract the FKO related to surface or interface we can determine the electric fields independently.

There are at least three methods of decomposing the PR signal into the surface and interface related ones. The first one takes advantage of the fact that we have two signals from different depths in the sample. In the case of PR signal consisting of two subsignals, from the surface region and from the interface one, the etching procedure changes only one part of the measured signal. The PR subsignal from the interface is changed due to the change in the distance between surface and interface. For such a case we can write

$$\left(\frac{\Delta R}{R}\right)_1 = \left(\frac{\Delta R}{R}\right)_S + A\left(\frac{\Delta R}{R}\right)_I, \tag{41}$$

$$\left(\frac{\Delta R}{R}\right)_2 = \left(\frac{\Delta R}{R}\right)_S + B\left(\frac{\Delta R}{R}\right)_I \tag{42}$$

where 1 and 2 represent the PR signals measured for as-grown sample and after etching, respectively, and S and I stand for signals from surface and interface, respectively. Following relations (41) and (42) we can determine the subsignal from interface as the difference between the spectra measured for as-grown and etched samples [87] − [89]. This subsignal is given with the accuracy of a constant factor, which is sufficient since PR spectra are usually given in the arbitrary units. In
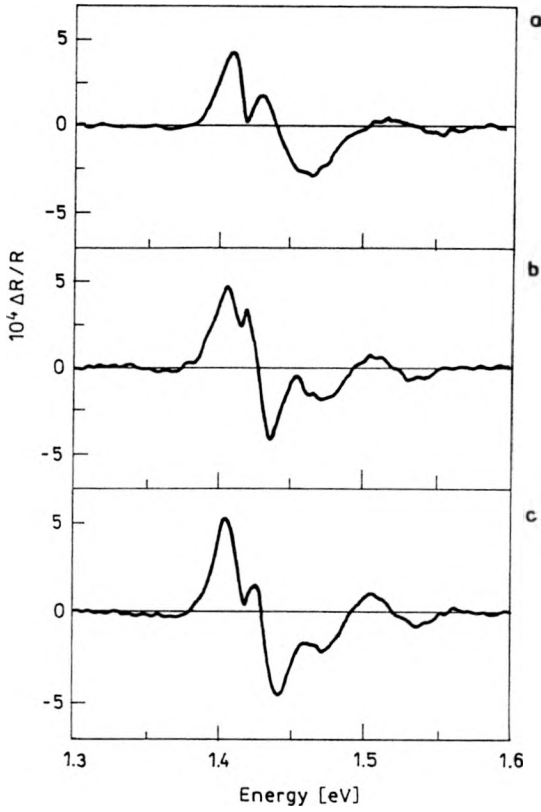
Fig. 21. The PR spectra for an *n*-type GaAs/SI GaAs structure [88]: **a** — before etching, **b** — after etching for 1 min, **c** — after next etching for 1 min.
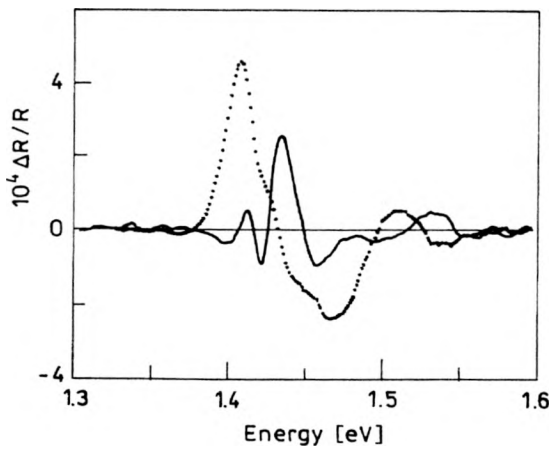

Fig. 22. PR spectra determined by the decomposition of the spectra shown in Fig. 21 into spectrum connected with the internal electric field in the surface region (dotted line) and the spectrum connected with the internal electric field in the interface region (solid line) [88].

Figure 21, an example of the PR spectra for GaAs/SI-GaAs homojuction, before etching and after two sequential etching procedures is plotted [88]. In Figure 22, the decomposition into subsignals from the surface and from the interface is shown.

A similar method may be used in the non-destructive mode when the etching procedure is replaced by the two PR measurements with two different wavelengths of the laser pump beam [27], [90] – [93]. In this case the situation can be even simpler. If one of the measured spectra is taken by using a very short wavelength of the laser, the signal is only from the surface (parameter A in Eq. (41) is equal to zero). Then the subsignal from the interface can be obtained by simple difference between PR signals obtained with longer and shorter laser wavelengths. An example in which this method is used is shown in Fig. 23 for the case of $Al_{0.11}Ga_{0.89}As$ layer grown on GaAs substrate [27].
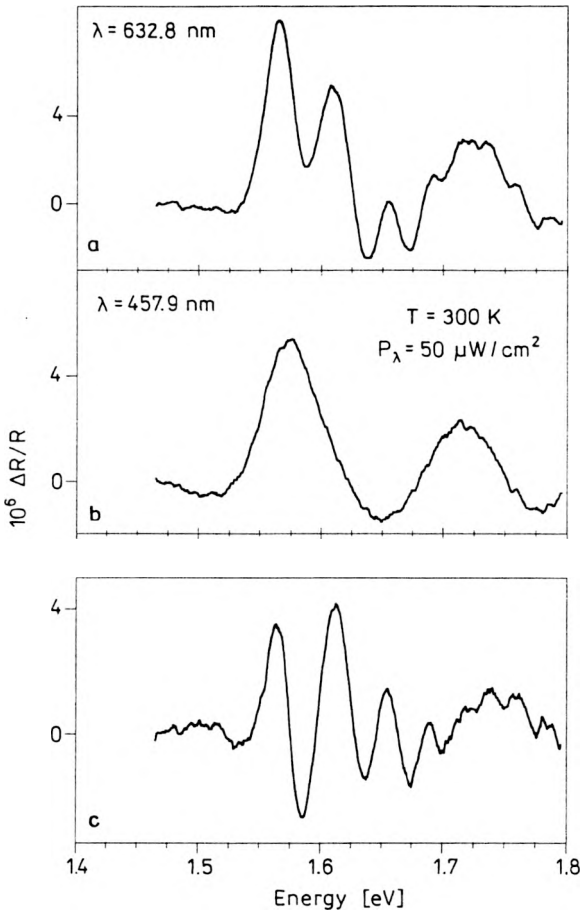

Fig. 23. PR spectra for $Al_{0.11}Ga_{0.89}As$ layers obtained using the following pump beams: **a** – 632.8 nm line of the He-Ne laser, **b** – 457.9 nm line of the Ar^+ laser, **c** – the difference between the two former spectra giving the Franz–Keldysh oscillations connected with the electric field at the $Al_{0.11}Ga_{0.89}As$/GaAs interface [27].

Another method of evaluating internal electric fields from the photoreflectance is the fast Fourier transformation (FFT) of the PR spectrum [94] − [99]. The FFT is applied to the PR spectra in the energy region higher than the band gap energy to obtain the FKO period and the electric field in the sample. We transform the x-axis variable from $\varepsilon = (E - E_g)^{3/2}$ to inverse of ε as τ, and the y-axis variable from $\Delta R/R$ to $G(\tau)$ that can be written as [97]

$$G(\tau) = \int (\Delta R/R) \exp(-i2\pi\varepsilon\tau) d\varepsilon. \tag{43}$$

The main peak τ_0 evaluated from the Fourier transform is related to the electric field by

$$\tau_0 = (2/3\pi)(2\mu)^{1/2}(1/ehF) \tag{44}$$

where μ is the reduced effective mass and F is the electric field [95]. While the peak position depends on the effective mass it is also possible to resolve the contribution from the light and heavy holes to the PR signal, if the contribution from the light holes is significant enough to be observed. An example of FFT of PR spectra is shown in Fig. 24 for the case of the structure consisting of doped (n and p doped) GaAs layer on SI GaAs substrate [98]. The two distinguished peaks, which can be seen, are related to the surface and interface electric fields.
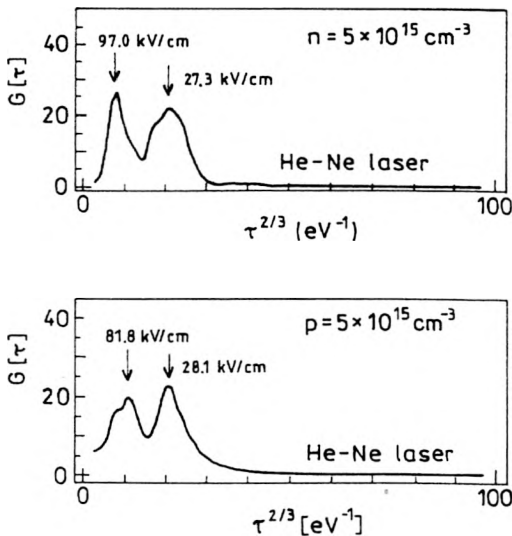

Fig. 24. FFT results of PR spectra consisting of two different periods FK ocillations for n and p-type GaAs layer on SI GaAs substrate [98].

The third, most recent method of subtracting signals from different parts of the sample is the phase suppression method [100] − [105]. In this method, advantage is taken of the fact that PR spectrum is commonly measured by the lock-in technique. It allows separation of the in-phase and out-phase (quadrature) components of the detected PR response. The different line shape of the in-phase and

the quadrature components can be understood by the following considerations [104]. The PR modulation under a square-wave pump is not a simple square wave (between two finite electric fields), but rather a complex wave form [100]. The output from the lock-in amplifier is the fundamental harmonic response

$$\frac{\Delta R(f_m, \Phi_{ref})}{R} = \text{Re}\left(e^{-i\Phi_{ref}}\frac{2}{T}\int_0^T \frac{\Delta R(t)}{R} e^{-2\pi i f_m t}\,dt\right) \tag{45}$$

where T is the period, Φ_{ref} is the reference phase with respect to the phase of the chopped laser beam, $\Phi_{ref} = 0$, and $\pi/2$ give the in-phase and out-phase components of the lock-in amplifier output, respectively. Under small modulation, Eq. (45) can be simplified to

$$\frac{\Delta R(E, f_m, \Phi_{ref})}{R} \sum_i L_i(E, F_i)\frac{1}{\sqrt{1+4\pi^2 f_m^2 \tau_i^2}}\cos(\Phi_{ref} - \Phi_i) \tag{46}$$

where $L_i(E, F_i)$ is the line shape at $f_m = 0$ for signal from the i-th region, F_i is the electric field, τ_i is the characteristic time constant, and Φ_i is the phase delay given by

$$\Phi_i = -\arctan(2\pi f_m \tau_i). \tag{47}$$

If the time constants associated with various regions of the samples are different, Eq. (46) yields a different line shape for the in-phase and out-phase signals. For example, a "slower" signal (larger τ_i) is more pronounced in the quadrature component, while a "faster" one is more pronounced in the in-phase component. Equation (46) also shows the possibility of suppressing one of the features (from the i-th region) by selecting $(\Phi_{ref} - \Phi_i) = \pi/2$ and the possibility to extract the other features (from the j-th region) as long as $\tau_j \neq \tau_i$.

It can be proven that

$$\frac{\Delta R(E, f_m, \Phi_{ref})}{R} = \frac{\Delta R(E, f_m, 0)}{R}\cos(\Phi_{ref}) + \frac{\Delta R(E, f_m, \pi/2)}{R}\sin(\Phi_{ref}) \tag{48}$$

where $\Delta R(E, f_m, 0)/R$ and $\Delta R(E, f_m, \pi/2)/R$ are the in-phase and quadrature components of the lock-in output, respectively. Therefore, the output in a lock-in amplifier can be represented as a vector in the reference phase space.

Figure 25 illustrates a vector representation of two signals (FKO–A and FKO–B) with different phase delays, the vector sum of which is shown by FKO–AB. Its projection on x- (y-) axis represents the in-phase (out-phase) signal. In a new reference phase frame Φ_{ref} with OX' perpendicular to FKO–B, the projection of FKO–B on OX' is zero while FKO–A still has significant projection on OX'. Therefore, FKO–B can be extracted.

It is important to note that it is not necessary to take many spectra at different phases to find this reference angle. In fact, only two measurements (in-phase and quadrature) are enough. Equation (48) can be used to generate a series of spectra at various angles, examine them, and pick one that suppresses one of the components. In Figure 26 the spectra of GaAs δ-doped sample are shown. In Figure 26c, there is
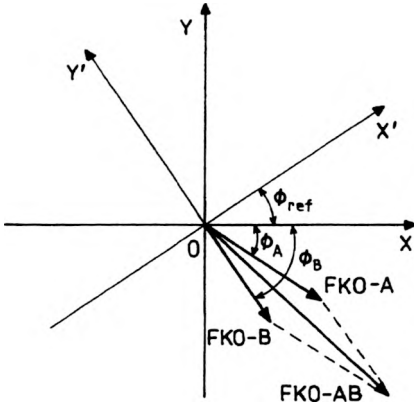
Fig. 25. Vector representation of the two FKO signals with different phase delay.
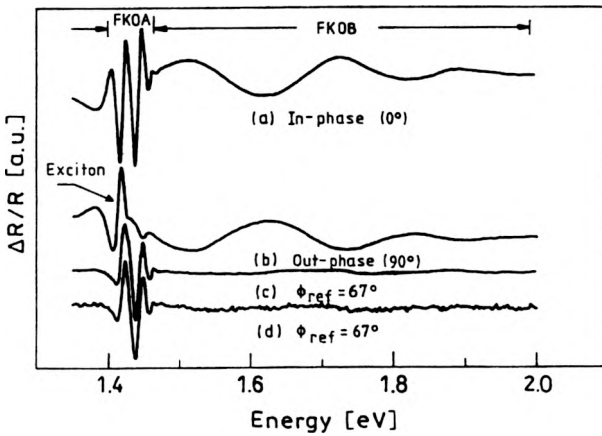

Fig. 26. Room temperature PR spectra from δ-doped GaAs sample [104], [105]: **a** — in-phase signal, **b** — out-phase signal, **c** — computer generated spectrum at a phase of $\Phi_{ref} = 67°$, **d** — experimental result from a re-scan at the same phase angle.

a computer-generated spectrum at $\Phi_{ref} = 67°$ using the in-phase and out-phase spectra of Figs. 26 a, b. In this case, the signal of the longer period FKOs disappears and the shorter-period FKOs remains. Also shown in Fig. 26d is the experimental result from a re-scan at a phase angle of $\Phi_{ref} = 67°$, which is in good agreement with the calculated line shape. This feature is designed as FKO–*A*. Using the in-phase and out-phase spectra again, we can find that FKO–*A* is suppressed at phase angle $\Phi_{ref} = 85°$. In this case the longer-period FKOs remain and are designated as FKO–*B*. From the reference phase which suppressed FKO–*A* (FKO–*B*) we can find that the phase delay for FKO–*A* (FKO–*B*) is $\Phi_A = -23°$ ($\Phi_B = -5°$). The characteristic time constants for FKO–*A* and FKO–*B* were deduced from Eq. (47) to be 70 and 340 μs, respectively. These time constants are related to limiting process of discharge and recharge of the surface/interface states, such as thermoionic emission

over the potential barriers, emission of charges from the surface/interface states/traps, *etc.* Since the density of the interface states in an MBE-grown sample is typically less than the density of the surface states, we can assign the fast process (FKO–*A*) to the buffer region, while the slower process (FKO–*B*) to the top region. The values of the electric fields can be obtained from the position of the FKO extrema in the "purified" spectra (see Sec. 3.2).

4.8. Influence of annealing, processing and growth conditions

Photoreflectance spectroscopy has become an effective tool to study various process and growth induced effects as well as the influence of annealing [90], [91], [106] – [116].

The PR has been used to the *in situ* study of the Fermi level pinning behaviour of *n*- and *p*-type GaAs (001) surfaces in the ultra-high vacuum environment of a molecular beam epitaxy chamber [108]. The effects of few monolayers of arsenic deposition/desorption have been investigated in UN$^+$ and UP$^+$ (highly doped layer on the undoped substrate) structures. In the UN$^+$ (UP$^+$) structures the barrier heights $V_{B,n}$ ($V_{B,p}$) are related to electric field F (as measured from FKO) by YIN *et al.* [106]

$$V_B = FL + \frac{kT}{q} + SCC \tag{49}$$

where the second and third terms are the Debye length and space charge layer corrections, respectively, L is the thickness of the doped layer. The surface Fermi level V_F is related to the measured barrier height V_B by

$$V_F = V_B + V_P \tag{50}$$

where V_P is the photovoltage. Typically, the value of V_P at 300 K is about 100 meV [106], [117].
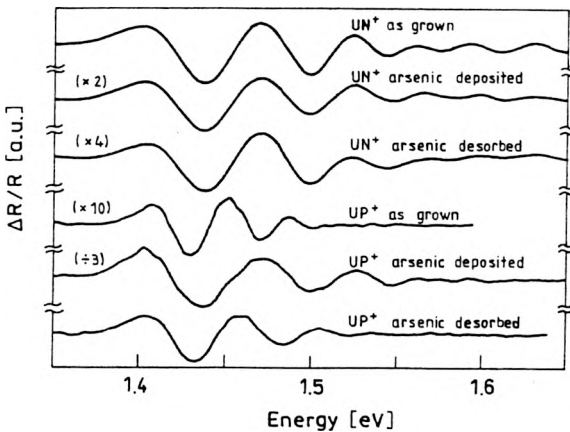

Fig. 27. *In situ* measured PR spectra for GaAs UN$^+$ and UP$^+$ structures for the cases of as-grown samples and after As deposition and desorption [108].
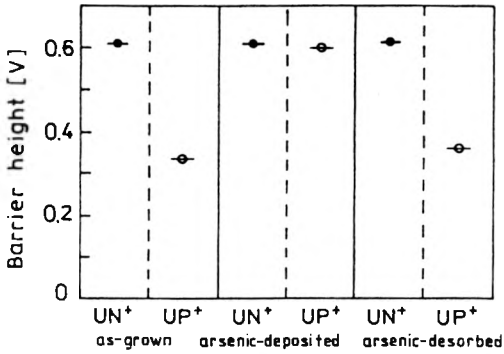
Fig. 28. Barrier heights $V_{B,n}$ (solid circles) and $V_{B,p}$ (open circles) determined from PR measurements for as-grown, arsenic-deposited and arsenic-desorbed situations [108].

Figure 27 shows the PR spectra of these UN$^+$ and UP$^+$ samples after arsenic deposition or desorption. The obtained barrier heights for all these cases are shown in Fig. 28.

The PR has also been used to study the effects of *in situ* substrate cleaning processes in GaAs homoepitaxial structures [112]. Figures 29 and 30 present the PR spectra of GaAs films on semi-insulating and n^+-doped GaAs substrates, respectively, for three different methods of the surface cleaning: annealing under the As$_4$ overpressure at a substrate temperature of 570 °C, the exposure to TDMAAs

▲
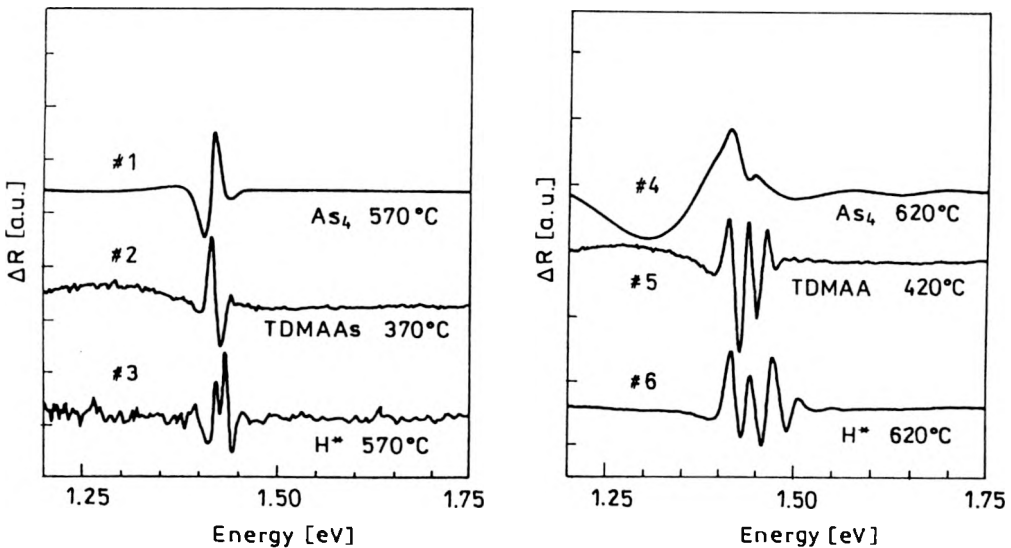
Fig. 29. Room temperature PR spectra for GaAs layers grown on semi-insulating substrates, for three different *in situ* substrate surface cleaning processes [112].

Fig. 30. Room temperature PR spectra for GaAs layers grown on n^+ substrates, for three different *in situ* substrate surface cleaning processes [112].

(trisdimethylaminoarsine) which is a reactive gas that slightly etches the substrate surface, and the cleaning by hydrogen radicals (H*). In Figures 31 and 32, the depth profiles of C and O from SIMS measurements are plotted for samples grown on semi-insulating and doped substrates, respectively.
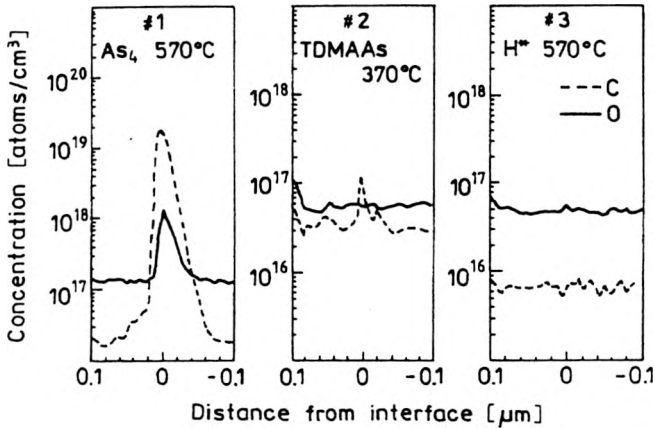

Fig. 31. SIMS depth profiles of C and O for samples grown on semi-insulating GaAs substrates [112].
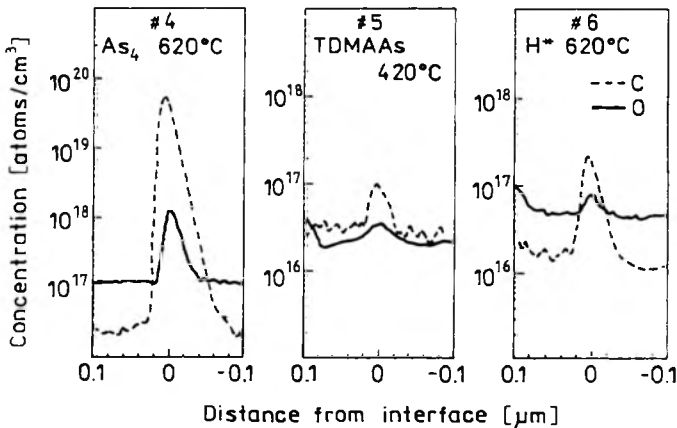

Fig. 32. SIMS depth profiles of C and O for samples grown on n^+ GaAs substrates [112].

Because of the accumulation of impurities at the substrate/epilayer interface, the generation of interfacial electric fields has a strong influence on the transport of carriers. The built-in electric fields have been evaluated from the FKO of the spectra from Figs. 29 and 30. A first glance shows that PR is indeed sensitive to the differences observed by SIMS. These differences are manifested, as expected, through FKO, which shows different characteristic. The PR spectrum in Fig. 29c corresponds to the sample with the lower amount of C and O impurities (Fig. 31c), then it is expected that the interfacial electric field is smaller than those present in the other

samples. Thus, in sample cleaned by H* they have obtained almost a flat-band condition at the interface. This yields a very low signal-to-noise ratio in the PR spectrum of this sample. As the content of impurities increases, the PR signal to noise ratio increases (see Figs. 29a, b). If the region close to the substrate/epi-layer interface is considered as an intrinsic-heavily doped junction, the charge density at this interface could be responsible for the rapid damping in FKO observed in Figs. 29a, b. For the samples grown on n^+-GaAs substrates, the slower damping of FKO for the spectra shown in Figs. 30b, c, could be due to the presence of a more uniform electric field, because of a larger band bending at the interface caused by n^+ substrate. The oscillations present in the PR spectrum shown in Fig. 30a do not follow the Franz–Keldysh model. This could be due to a short of interference effect, which shows up for highly doped samples during the modulation process.
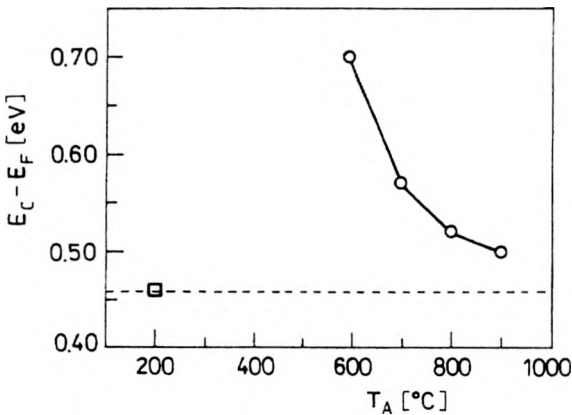

Fig. 33. Fermi level of annealed low temperature GaAs as a function of the annealing temperature determined from PR measurements [113]. For comparison, the Fermi level of 200 °C grown low temperature GaAs is shown (dashed line).

The PR has also been used to study the Fermi level of annealed low-temperature grown GaAs in sample structures composed of low-temperature GaAs on top of Si-δ-doped GaAs. The plot of the Fermi level as a function of annealing temperature obtained from PR for this sample is shown in Fig. 33. The decrease in the Fermi level at higher annealing temperatures can be explained with the buried Schottky barrier model. For sample annealed at 600 °C, the TEM image shows a high density of As precipitates. This high precipitate density causees the overlapping of the depletion regions between the internal Schottky barriers. Consequently, the Fermi level is pinned near the mid-gap. When samples have been annealed at higher temperatures, the precipitates increased in size but decreases in density. The decrease of precipitate density reduced the overlap of the depletion regions between the internal Schottky barriers. This makes it possible to decrease the Fermi level with the increase in the annealing temperature.

5. Summary

We have reviewed the experimental, theoretical and instrumentation details that occur in photoreflectance spectroscopy. The PR is extremely useful since it is not only contactless but requires no special mounting of the sample. It can be utilised under a wide variety of conditions such as elevated temperatures, including *in situ* monitoring of growth, in the restrictive environment of a diamond anvil cell for uniaxial stress studies. The emphasis of this work has been placed on investigating the properties of semiconductor bulk and simple structures, mainly in relation to the electronic band structure. Refined theories, particularly the low-field third derivative formulation and the Franz–Keldysh model of electromodulation, enabled investigators to quantitatively analyse the photoreflectance spectra. The sharp, derivative like features of photomodulated signals made it possible to conveniently investiagte the band structure of a wide variety of semiconductors and to explore the influence of different perturbations like temperature, strain, built-in electric field, growth, processing and annealing effects. Also, there is more information to be gained from pump frequency, amplitude and wavelength dependence. The problem of the spurious background signal has been reduced or eliminated, *e.g.*, by making use of double monochromator or double detector system, dye laser as a probe beam or sweeping PR.

References

[1] PHILLIP H. R., EHRENREICH H., Phys. Rev. **129** (1963), 1550.
[2] ASPNES D. E., STUDNA A. A., Phys. Rev. B **7** (1973), 4605.
[3] POLLAK F. H., [In] *Handbook on Semiconductors*, Vol. 2, [Ed.] M. Balkanski, North-Holland, Amsterdam 1994, p. 527.
[4] CARDONA M., *Modulation Spectroscopy*, Academic Press, New York 1969.
[5] ASPNES D. E., [In] *Handbook on Semiconductors*, Vol. 2, [Ed.] M. Balkanski, Amsterdam 1980, p. 109.
[6] GLEMBOCKI O. J., SHANABROOK B. V., [In] *Semiconductors and Semimetals*, Vol. 67, [Ed.] D. Seiler, Academic Press, New York 1992, p. 222.
[7] MISIEWICZ J., JEZIERSKI K., SITAREK P., MARKIEWICZ P., KORBUTOWICZ R., PANEK M., ŚCIANA B., TŁACZAŁA M., Adv. Mater. Opt. Electron. 5 (1995), 321.
[8] SHEN H., POLLAK F. H., WOODALL J. M., SACKS R. N., J. Electron. Mater. 19 (1990), 283.
[9] THEIS W., SANDERS M., LEAK G. D., BAJAJ C. E., MORKOÇ H., Phys. Rev. B 37 (1988), 3042.
[10] SHANABROOK B. V., GLEMBOCKI O. J., BEARD W. T., Phys. Rev. B 35 (1987), 2540.
[11] GLEMBOCKI O. J., SHANABROOK B. V., Proc. SPIE 794 (1987), 74.
[12] MARKIEWICZ P., Report of the Institute of Physics, Wrocław Universty of Technology, (in Polish), SPR No. 287, Wrocław 1995.
[13] SHEN H., DUTTA M., Appl. Phys. Lett. 57 (1990), 587.
[14] SYDOR M., BADAKHSHAN A., J. Appl. Phys. 70 (1991), 2322.
[15] SERAPHIN B. O., BOTTKA N., Phys. Rev. 145 (1966), 628.
[16] ASPNES D. E., Surface Sci. 37 (1973), 418.
[17] POLLAK F. H., GLEMBOCKI O. J., Proc. SPIE 946 (1988), 2.

[18] GLEMBOCKI O. J., SHANABROOK B. V., Superlatt. Microstruct. 5 (1989), 603.
[19] ASPNES D. E., ROWE J. E., Pyhs. Rev. B 5 (1972), 4022.
[20] SHEN H., POLLAK F. H., Phys. Rev. B 42 (1990), 7097.
[21] MISIEWICZ J., ZHENG X. L., BECLA P., HEIMAN D., Solid State Commun. 66 (1988), 351.
[22] ISHITNI Y., HAMADA H., MINAGAWA S., YAGUCHI H., SHIRAKI Y., Jpn. J. Appl. Phys. 36 (1997), 6607.
[23] SHIRAKATA S., CHICHIBU S., ISOMURA S., Jpn. J. Appl. Phys. 36 (1997), 7160.
[24] *Ibidem* p. 6645.
[25] SHAN W., LITTLE B. D., SONG J. J., FENG Z. C., SHURMAN M., STALL R. A., Appl. Phys. Lett. 69 (1996), 3315.
[26] SITAREK P., MISIEWICZ J., VEJE E., Proc. SPIE 3725 (1999).
[27] SITAREK P., MISIEWICZ J., VEJE E., Adv. Mater. Opt. Electron., in press.
[28] EL ALLALI M., SORENSEN C. B., VEJE E., TIDEMAND-PETERSSON P., Phys. Rev. B 48 (1993), 4398.
[29] PETERS L., PHANEUF L., KAPITAN L. W., THEIS W. M., J. Appl. Phys. 62 (1987), 4558.
[30] LEE C., LEE N. Y., KIM J. E., PARK H. Y., KWAK D. H., LEE H. C., LIM H., J. Appl. Phys. 77 (1995), 6727.
[31] JEZIERSKI K., SITAREK P., MISIEWICZ J., PANEK M., ŚCIANA B., KORBUTOWICZ R., TŁACZAŁA M., Vacuum 48 (1997), 277.
[32] ZHANG X., CHUA S. J., LIU W., CHONG K. B., Appl. Phys. Lett. 72 (1998), 1890.
[33] BADAKHSHAN A., GLOSSER R., LAMBERT S., J. Appl. Phys. 69 (1991), 2525.
[34] KALLERGI N., ROUGHANI B., AUBEL J., SUNDARAM S., J. Appl. Phys. 68 (1990), 4656.
[35] LIPSANEN H. K., AIRAKSINEN V. M., Appl. Phys. Lett. 63 (1993), 2863.
[36] HUANG D., MUI D., MORKOÇ H., J. Appl. Phys. 66 (1989), 358.
[37] GHOSH S., ARORA B., J. Appl. Phys. 81 (1997), 6968.
[38] AMIRTHARAJ P. M., DINAN J. H., KENNEDY J. J., BOYD J. R., GLEMBOCKI O. J., J. Vac. Sci. Technol. A 4 (1986), 2028.
[39] KSENDZOV A., POLLAK F. H., AMIRTHARAJ P. M., WILSON J. A., J. Cryst. Growth 86 (1988), 586.
[40] SHEN H., HANG Z., PAN S. H., POLLAK F. H., WOODALL J. M., Appl. Phys. Lett. 52 (1988), 2058.
[41] SHEN H., POLLAK F. H., WODDAL J. M., SACKS R. N., J. Vac. Sci. Technol. B 7 (1989), 804.
[42] KANATA T., MATSUNAGA M., TAKAKAWA H., HAMAKAWA Y., NISHINO T., J. Appl. Phys. 69 (1991), 3691.
[43] NAHORY R. E., SHAY J. L., Phys. Rev. Lett. 21 (1968), 1569.
[44] SHEN H., DUTTA M., LUX R., BUCHWALD W., FOTIADIS L., SACKS R. N., Appl. Phys. Lett. 59 (1991), 321.
[45] MOSS S. C., KNUDSEN J. F., BOWMAN R. C., ADAMS P. M., SMITH D. D., Appl. Surface Sci. 50 (1991), 337.
[46] TANI M., SAKAKI K., ABE H., NAKASHIMA S., HARIMA H., HANGYO M., TOKUDA Y., KANAMOTO K., ABE Y., TSUKADA N., Jpn. J. Appl. Phys. 33 (1994), 4807.
[47] ABE H., HARIMA H., NAKASHIMA S., TANI M., Jpn. J. Appl. Phys. 35 (1996), 5955.
[48] YU J. S., HORNG S., CHI C. C., Jpn. J. Appl. Phys. 36 (1997), 2144.
[49] *Ibidem*, 37 (1998), 554.
[50] SAKAI M., SHINOHARA M., J. Phys. Soc. Jpn. 66 (1997), 738.
[51] SAKAI M., SHINOHARA M., Appl. Surface Sci. 113/114 (1997), 523.
[52] LAN S., CHEN Z. Y., XU W. J., YANG C. Q., LIU H. D., Solid State Commun. 93 (1995), 497.
[53] PAMPALONA PIRES M., SOUZA P. L., VON DER WEID J. P., Appl. Phys. Lett. 65 (1994), 88.
[54] LAUTENSCHLAGER P., CARRIGA M., CARDONA M., Phys. Rev. B 35 (1987), 9174.
[55] *Ibidem*, 36 (1987), 4813.
[56] MANOOGIAN A., WOOLLEY J. C., Can. J. Phys. 62 (1984), 285.
[57] RÖPPISCHER H., STEIN N., BEHN U., NOVIKOV A. B., J. Appl. Phys. 76 (1994), 4340.
[58] HANG Z., SHEN H., POLLAK F. H., Solid State Commun. 73 (1990), 15.
[59] POLLAK F. H., Proc. SPIE 1361 (1991), 109.
[60] HANG Z., YAN D., POLLAK F. H., PETTIT G. D., WOODALL J. M., Phys. Rev. B 44 (1991), 10546.
[61] CHEN J. H., CHI W. S., HUANG Y. S., YIN Y., POLLAK F. H., PETTIT G. D., WOODALL J. M., Semicond. Sci. Technol. 8 (1993), 1420.

[62] CHI W. S., HUANG Y. S., QIANG H., POLLAK F. H., PETTIT D. G., WOODALL J. M., Jpn. J. Appl. Phys. **33** (1994), 966.
[63] KUAN H., SU Y. K., WU T. S., HUANG Y. S., CHI W. S., Solid State Electron. **39** (1996), 885.
[64] BOUAMAMA K., HÖRIG W., NEUMANN H., Semicond. Sci. Technol. **13** (1998), 75.
[65] BELLANI V., AMIOTTI M., GEDDO M., GUIZZETTI G., LANDGREN G., Mat. Res. Soc. Symp. Proc. **324** (1994), 225.
[66] GEDDO M., BELLANI V., GUIZETTI G., Phys. Rev. B **50** (1994), 5456.
[67] PAL U., HERRERA PEREZ J. L., PIQUERAS J., DIEGUEZ E., Mater. Sci. Eng. B **42** (1996), 297.
[68] SHEN S. C., ZHANG L. J., LU W., BICKNELL-TASSIUS R. N., Solid State Electron. **37** (1994), 1087.
[69] LIN C. H., SINGER K. E., EVANS-FREEMAN J. H., HEATH K., MISSOUS M., Semicond. Sci. Technol. **12** (1997), 1619.
[70] LI C. F., HUANG Y. S., MALIKOVA L., POLLAK F. H., Phys. Rev. B **55** (1997), 9251.
[71] SHEN H., PAN S. H., HANG Z., LENG J., POLLAK F. H., WOODALL J. M., SACKS R. N., Appl. Phys. Lett. **53** (188), 1080.
[72] QIANG H., POLLAK F. H., SOTOMAYOR TORRES C. M., LEITH W., KEAN A. H., STROSCIO M. A., IAFRATE G. J., KIM K. W., Appl. Phys. Lett. **61** (1992), 1411.
[73] GLEMBOCKI O. J., Mater. Res. Soc. Symp. Proc. **160** (1990), 631.
[74] SĘK G., TALIK S., MISIEWICZ J., RADZIEWICZ D., TŁACZAŁA M., PANEK M., KORBUTOWICZ R., Electron. Technol. **30** (1997), 366.
[75] SĘK G., MISIEWICZ J., RADZIEWICZ D., TŁACZAŁA M., PANEK M., KORBUTOWICZ R., Vacuum **50** (1998), 219.
[76] FITZGERALD E. A., [In] *Properties of lattice-matched and strained indium galium Arsenids*, [In] IEE EMIS Derivarives Ser. 8, [Ed.] P. Bhattacharaya, 1993, p. 6.
[77] ANDREANI L. C., DE NOVA D., DI LERNIA S., GEDDO M., GUIZETTI G., PATRINI M., BOCCHI C., BOSACCHI A., FRENCHI S., J. Appl. Phys. **78** (1995), 6745.
[78] RADHAKRISHNAN K., YOON S. F., LI H. M., HAN Z. Y., ZHANG D. H., J. Appl. Phys. **76** (1994), 246.
[79] MO S., PEINER E., BARTLES A., TANG G. P., SCHLACHETZKI A., KUZMENKO R., HILDEBRANDT S., SCHREIBER J., Jpn. Appl. Phys. **35** (1996), 4238.
[80] LEE J. H., JANG K. S., SHIN C. S., PARK H. L., KIM T. W., J. Appl. Phys. **75** (1994), 8216.
[81] HAN M. S., KANG T. W., KIM T. W., Solid State Commun. **105** (1998), 709.
[82] CHICHIBU S., SHIKANAI A., AZUHATA T., SOTA T., KURAMATA A., HORINO K., NAKAMURA S., Appl. Phys. Lett. **68** (1996), 3766.
[83] TCHOUNKEU M., BRIOT O., GIL B., ALEXIS J. P., AULOMBARD R. L., J. Appl. Phys. **80** (1996), 5352.
[84] SHIKANAI A., AZUHATA T., SOTA T., CHICHIBU S., KURAMATA A., HORINO K., NAKAMURA S., J. Appl. Phys. **81** (1997), 417.
[85] ALEMU A., GIL B., JULIER M., NAKAMURA S., Phys. Rev. B **57** (1998), 3761.
[86] QIANG H., POLLAK F. H., HICKMAN G., Solid State Commun. **76** (1990), 1087.
[87] WANG D. P., SHEN T. L., Jpn. J. Appl. Phys. **33** (1993), 1253.
[88] JEZIERSKI K., MISIEWICZ J., MARKIEWICZ P., PANEK M., ŚCIANA B., TŁACZAŁA M., KORBUTOWICZ R., Phys. Status Solidi **147** (1995), 467.
[89] JEZIERSKI K., SITAREK P., MISIEWICZ J., PANEK M., ŚCIANA B., KORBUTOICZ R., TŁACZAŁA M., Vacuum **48** (1997), 277.
[90] WANG Z., PAN S., HUANG S., ZHANG C., MU S., ZHOU X., JIAN J., XU G., CHEN Z., J. Phys. D: Appl. Phys. **26** (1993), 1493.
[91] WANG Z., PAN S., MU S., Phys. Status Solidi **140** (1993), 135.
[92] JEZIERSKI K., SITAREK P., MISIEWICZ J., PANEK M., ŚCIANA B., KORBUTOWICZ R., TŁACZAŁA M., Acta Phys. Pol. A, **88** (1995), 751.
[93] YOSHITA M., TAKAHASHI T., Appl. Surface Sci. **115** (1997), 347.
[94] SCHEIBLER H. E., ALPEROVICH V. L., JAROSHEVICH A. S., TEREKHOV A. S., Phys. Status Solidi A **152** (1995), 113.
[95] WANG D. P., CHEN C. T., Appl. Phys. Lett. **67** (1995), 2069.
[96] WANG D. P., CHEN C. C., SHEN T. L., HSU T. M., LEE W. C., J. Appl. Phys. **80** (1996), 6980.

[97] NUKAEW J., MATSUBARA N., FUJIWARA Y., TAKEDA Y., Appl. Surface Sci. **117/118** (1997), 776.

[98] NUKAEW J., FUJIWARA Y., TAKEDA Y., Jpn. J. Appl. Phys. **36** (1997), 7019.

[99] CHANG W. H., HSU T. M., LEE W. C., CHUANG R. S., J. Appl. Phys. **88** (1998), 7873.

[100] SHEN H., DUTTA M., J. Appl. Phys. **78** (1995), 2151.

[101] HILDEBRANDT S., MURTAGH M., KUZMENKO R., KIRCHER W., SCHREIBER J., Phys. Status Solidi A **152** (1995), 147.

[102] NOVIKOV A. B., RÖPPISCHER H., STEIN N., NOVIKOV B. V., J. Appl. Phys. **78** (1995), 4011.

[103] SCHREIBER J., KIRCHNER W., HILDEBRANDT S., GANSHA A., KUZMENKO R., [In] *Highlights of Light Spectroscopy on Semiconductors*, [Ed.] A. D'Andrea, L. G. Quagliano, S. Selci, World Sci., Singapore 1996, p. 29.

[104] TYAN S. L., WANG Y. C., HWAN J. S., SHEN H., Appl. Phys. Lett. **68** (1996), 3452.

[105] WANG Y. C., CHOU W. Y., HWANG W. C., HWANG J. S., Solid State Commun. **104** (1997), 717.

[106] YIN X., CHEN H. M., POLLAK F. H., CHAN Y., MONTANO P. A., KIRCHNER P. D., PETTIT G. D., WOODALL J. M., J. Vac. Sci. Technol. A **10** (1992), 131.

[107] OH Y. T., BYUN S. C., LEE B. R., KANG T. W., HONG C. Y., PARK S. B., LEE H. K., KIM T. W., J. Appl. Phys. **76** (1994), 1959.

[108] YAN D., POLLAK F. H., CHIN T. P., WOODALL J. M., Phys. Rev. B **52** (1995), 4674.

[109] NAKANISHI H., WADA K., WALUKIEWICZ W., J. Appl. Phys. **78** (1995), 5103.

[110] MOCHIZUKI Y., ISHII T., MIZUTA M., MOCHIZUKI A., LANGER J. M., Phys. Rev. Lett. **77** (1996), 3601.

[111] RIGHINI M., FERRARI L., FODONIPI M., SELCI S., ALMEIDA J., COLUZZA C., [In] *Highlights of Light Spectroscopy on Semiconducors*, [Ed.] A. D'Andrea, L. G. Quagliano, S. Selci, World Sci., Singapore 1996, p. 113.

[112] LOPEZ-LOPEZ M., MELENDEZ-LIRA M., GOTO S., Appl. Phys. Lett. **71** (1997), 338.

[113] LEE W. C., HSU T. M., WANG S. C., CHANG M. N., CHYI J. I., J. Appl. Phys. **83** (1998), 486.

[114] BADAKHSHAN A., ENGLAND J. L., THOMPSON P., CHEUNG P., YANG C. H., ALAVI K., J. Appl. Phys. **81** (1997), 910.

[115] GLEMBOCKI O. J., TUICHMAN J. A., DAGATA J. A., KO K. K., PANG S. W., STUTZ C. E., Appl. Phys. Lett. **73** (1998), 114.

[116] PAGET D., KIERREN B., HOUDRÉ R., J. Vac. Sci. Technol. A **16** (1998), 2350.

[117] YAN D., LOOK E., YIN X., POLLAK F. H., WOODALL J. M., Appl. Phys. Lett. **65** (1994), 186.